Particle sources and downward fluxes in the Eastern Fram Strait under the influence of the West Spitsbergen Current

Anna Sanchez-Vidal[1*], Oriol Veres[1], Leonardo Langone[2], Benedicte Ferré[3], Antoni Calafat[1], Miquel Canals[1], Xavier Durrieu de Madron[4], Serge Heussner[4], Jurgen Mienert[3], Joan O. Grimalt[5], Antonio Pusceddu[6], Roberto Danovaro[6]

[1] GRC Geociències Marines, Departament d'Estratigrafia, Paleontologia i Geociències Marines, Universitat de Barcelona, Barcelona, Spain.

[2] CNR-ISMAR, Istituto Scienze Marine, Bologna, Italy.

[3] CAGE—Centre for Arctic Gas Hydrate, Environment and Climate, Department of Geology, University of Tromsø, Tromsø, Norway.

[4] CEFREM, UMR CNRS 5110, CNRS - Univ. Perpignan, Perpignan, France.

[5] Institut de Diagnosi Ambiental i Estudis de l'Aigua (IDAEA), CSIC, Barcelona, Spain

[6] Department of Life and Environmental Sciences, Polytechnic University of Marche, Ancona, Italy.

* Corresponding author. Tel: +34934021361; Fax: +34934021340. E-mail address: anna.sanchez@ub.edu (Anna Sanchez Vidal)

Keywords: Particle fluxes, Organic Carbon, Ice Rafted Detritus, West Spitsbergen Current, Fram Strait

Highlights:

- Downward flux of particles in the western Spitsbergen margin during one year is reported
- Particle fluxes and especially carbon fluxes are strongly sensitive to environmental conditions
- The West Spitsbergen Current resuspended and transported sediments northwards
- Settling of sea ice-transported IRDs impacted sedimentary and carbon dynamics in winter
- Pelagic settling of marine carbon represented < 28% of the carbon reaching annually the seafloor

Abstract

Dramatic losses of sea ice in the Arctic have been observed since the end of the 70s. In spite of the global importance of this process that likely witness significant modifications due to climate change, its impact on the carbon cycle of the Arctic has been poorly investigated. Information on organic carbon sources and export, redistribution procesess and burial rates in relation to climate change is needed, particularly in the Arctic land-ocean boundaries. Natural drivers that control downward fluxes of particles including carbon to the deep-sea floor are investigated with four moorings including sediment traps and currentmeters at the Arctic gateway in the eastern Fram Strait, which is the area where warm anomalies are transported northwards to the Arctic. Particles fluxes were collected over one year (July 2010 - July 2011) and have been analysed to obtain the content of the lithogenic fraction, calcium carbonate, organic carbon and its stable isotopes, opal, and the grain size. Records of near bottom current speed and temperature along with satellite observations of sea ice extent and chlorophyll-a concentration have been used for evaluation of the environmental conditions.

We found increased lithogenic fluxes (up to 9872 mg m^{-2} d^{-1}) and coarsening grain size of settling particles in late winter – early spring at the same time than intensification of the northwards flowing West Spitsbergen Current (WSC). The WSC was able to resuspend and transport northwards sediments that were deposited at the outlet of Storfjordrenna and on the upper slope west of Spitsbergen. The signal of recurrent winnowing of fine particles was also detected in the top layer of surface sediments. In addition, an increased arrival of sea ice transported ice rafted detritus (> 414 detrital carbonate mineral grains larger than 1 mm per m^2) from the southern Spitsbergen coast along with terrestrial organic matter was observed beyond 1000 m of water depth during winter months. Finally, the downward particle fluxes showed typical seasonal cycle for high latitudes, with high percentages of the biogenic compounds (opal, organic carbon and calcium carbonate) linked to the typical phytoplankton bloom in spring - summer. However, on an annual basis local planktonic production was a secondary source for the downward OC, since most of the OC was advected laterally by the WSC. Overall,

these observations demonstrated the sensitivity of the downward flux of particles to environmental conditions such as hydrodynamics, sea ice rafting, and pelagic primary production. It is hypothesized that future alteration of the patterns of natural drivers due to climate change will probably lead to major shifts in the downward flux of particles, including carbon, to the deep sea ecosystems.

1. Introduction

During recent decades, extensive decrease in sea-ice extent and thickness have been reported in the Arctic (Parkinson et al., 1999; Vinje, 2001; Comiso et al., 2008; Gerland et al., 2008). In particular, sea ice extent in the Arctic shrank at a rate up to 10% per decade after 1996 and there was a massive reduction of ice extent in summer 2007 resulting in a minimum of only 4.1 million km^2 (Wadhams, 2013). This is an unequivocal sign for climate change (Intergovernmental Panel on Climate Change, 2001, 2007, 2013) and has raised severe concerns for the vast environmental and economic costs of melting Arctic ice (Whiteman et al., 2013). Alterations of seawater salinity, temperature and nutrient distribution may have resulted in changes to marine Arctic ecosystems at all levels of the trophic network (Wassmann et al., 2011), including the distribution and cycling of carbon (MacGilchrist et al., 2014). A recent study carried out in summer 2012, when Arctic sea ice declined to a record minimum of 3.4 million km^2, revealed a huge export of organic material of algal origin (up to 9 g m^{-2} y^{-1}) towards the sea bottom (Boetius et al., 2013). As climate models predict decreasing sea-ice thickness and nearly sea ice free summers (with some sea ice refuges in the region north of the Canadian Archipelago and Greenland) in the Arctic in the forthcoming decades (Wang and Overland, 2009), increasing inputs of organic material to the deep sea in the Arctic could be expected (Boetius et al., 2013). Because most benthic communities inhabiting the deep sea floor are dependent on sinking or advection of particulate organic carbon (McClain et al., 2012), and also because processes occurring in the Arctic impact the biogeochemical cycles on a global

86 scale (Carroll and Carroll, 2003), it is essential to investigate the sensitivity of natural drivers
87 and deep-sea ecosystem functioning to climate variability.

88 Our study investigates the spatial and temporal patterns of downward particle fluxes at the
89 transition zone between the North Atlantic and the Arctic Ocean on the western margin off
90 Spitsbergen, which is the largest island of the Svalbard archipelago. This area is very important
91 with regard to heat and water exchange because warm and salty Atlantic Water transported at
92 intermediate depths (~150 - 900m) toward the north is believed to contribute in shaping the
93 Arctic Ocean' ice cover (Polyakov et al., 2012a), which in turn is expected to trigger a number
94 of tipping elements (physical, chemical, and biological) with potentially large impacts in the
95 Arctic marine ecosystems (Duarte et al., 2012). In the present paper we explore the relationship
96 between hydrodynamic conditions, sea ice extent, primary production, and the total mass fluxes
97 and their composition (including the lithogenic fraction, calcium carbonate, organic carbon and
98 its stable isotopes, biogenic opal, and grain size). This research has been framed within the
99 HERMIONE (Hotspot Ecosystem Research and Man's Impact on European Seas) project from
100 the European Commission's FP7 programme, which set out to investigate the human impact
101 (through the indirect effects of climate change) on critical sites of Europe's deep-ocean margins.

102

103 **2. Study area**

104 The study area is located on the western margin off Spitsbergen, Svalbard Islands, in the south-
105 eastern Fram Strait where the Nordic Seas and the Arctic Ocean connect (Fig. 1).
106 Oceanographic conditions are characterized by the northward inflow of the West Spitsbergen
107 Current (WSC), constituting the northernmost extension of the Norwegian Atlantic Current
108 (Aagaard et al., 1987) carrying warm Atlantic Water (AW) into the Arctic Ocean (Manley,
109 1995). At about 79ºN the WSC splits into two branches, the east branch following the perimeter
110 of the Svalbard Islands and flowing southwards forming the East Spitsbergen Current, and the
111 west branch flowing southwards joining the East Greenland Current (EGC) in the western Fram

Strait (Quadfasel et al., 1987). While the WSC transports large quantities of heat poleward, the main ice outflow from the Arctic occurs in the EGC (Schlichtholz and Houssais, 2002).

The warm and saline AW loses heat and salt northward due to surface heat exchange with the atmosphere and mixing with ambient, fresher and colder waters (Saloranta and Haugan, 2004), largely coming from the fjords. Indeed, fjords in west Spitsbergen can be regarded as coastal polynyas, as the prevailing easterly (offshore) winds over the island lead to a significant cooling of the open water in the fjord (Skogseth et al., 2004) and ice growth. This triggers an increase in the salinity and density of the ambient waters and convection, eventually reaching the bottom. Dense water formation due to large polynya events in winter in Storfjorden and Isfjorden ultimately controls the exchange between the fjord and the shelf areas (Nilsen et al., 2008). The dense water produced in the fjords eventually overflows the sill and can reach deep into the Fram Strait (Fer et al., 2008).

The extent of ice-cover in the study area shows a pronounced seasonal cycle. The northern sector of the Svalbard archipelago is intersected by sea ice (known as the Marginal Ice Zone, MIZ) each year around March when sea ice covers most of the Barents Sea, while the sea ice extent is minimum in September. Despite high interannual variability, largest reductions in sea ice extent have been observed in the Barents Sea over the last few decades (Vinje, 2001; Gerland et al., 2008). In addition, land-fast sea ice develops in the Spitsbergen fjords in winter and spring, which starts melting in late spring.

The timing and magnitude of phytoplankton blooms in this region is linked to nutrient input by the inflowing AW and nutrient consumption during the summer productive period, and stratification vs. vertical mixing during winter. The phytoplankton spring bloom usually occurs in April-May with the increase in photosynthetically-active radiation, the decrease of the mixed layer depth, and the ice-melt induced stratification (Loeng, 1991; Wassmann et al., 2006), and is mainly dominated by diatoms and flagellates (Owrid et al., 2000; Richardson et al., 2005; Carmack and Wassman, 2006). In addition, phytoplankton blooms may develop under the ice over the nutrient-rich shelves of Spitsbergen (Arrigo et al., 2012). Zooplankton communities,

mainly herbivorous copepods of Atlantic or Arctic origin, graze on phytoplankton stocks and feed large populations of fish, sea birds and marine mammals (Wassman et al., 2006).

3. Material and Methods

3.1. Remote sensing

Daily sea ice concentrations have been provided by the National Snow and Ice Data Centre (NSIDC) from the Advanced Microwave Scanning Radiometer - Earth Observing System (AMSR-E) sensor on NASA's Aqua satellite. Maximum and minimum sea ice extents have been calculated from the sea ice concentration dataset by applying the ARTIST Sea Ice (ASI) algorithm (Spreen et al., 2008).

Monthly chlorophyll-a (hereinafter chl-a) concentration, with a 4 km resolution, has been obtained by the Moderate Resolution Imaging Spectroradiometer (MODIS) on Aqua satellite. Analyses and visualizations used have been produced with the Giovanni online data system, developed and maintained by the NASA GES DISC.

3.2. Data and sample collection

Four moorings were deployed from 23 July 2010 to 13 July 2011 at 1040 m (station A, ~1000 m), 1121 m (station D, ~1120 m), 1500 m (station B), and 2011 m (station C, ~2000 m) of water depth along the western margin of Spitsbergen in the eastern Fram Strait (Fig. 1). Stations A, B and C were equipped with one Technicap PPS3 sequential sampling sediment trap (12 collecting cups, 0.125 m^2 opening) at 25 m above the bottom (mab) collecting 1 sample per month. Mooring B had an extra trap at 975 m (hereinafter ~1000 m or 500 mab, B-Top). Mooring D was equipped with a McLane sequential sampling sediment trap (13 collecting cups, 0.5 m^2 opening) at 25 mab. The sample cups of the traps were filled up before deployment with a buffered 5% (v/v) formaldehyde solution in 0.45 μm filtered arctic seawater.

Each mooring included an Aanderaa currentmeter (RCM7/9) 2 m below the sediment trap recording current speed and direction, temperature and pressure with a sampling interval of 1

hour. Stations A, B and D also included a SBE 16 or 37-SMP recording temperature, salinity and pressure at 20-minute intervals at the sediment trap depth near the bottom. Unfortunately, RCM9 currentmeters at stations A, C and D failed due to water leakage, the compass of the near-bottom RCM7 currentmeter at station B was blocked, and the conductivity record at station D was unrealistic. Hence concomitant current amplitude and temperature were solely recorded at ~1000 and ~1500 m at station B. Near bottom temperature/salinity measurements were solely collected at stations A and B. In addition, CTD and turbidity profiles were collected with a SBE 911Plus probe next to the mooring sites during the deployment (23 July 2010) and the recovery (13 July 2011) of the moorings. Additional currentmeter observations collected by the Alfred Wegener Institute on the Fram Strait continental slope at 78°50' N (~300 km north of our study area) were used to complement the description of the WSC variability. We make use of data from mooring F4 at 1435 m water depth (Beszczynska-Möller et al., 2012a) and F5 at 2440 m water depth (Beszczynska-Möller et al., 2012b) (Fig. 1a).

Seabed sediment sampling was performed at each station, including an extra-station at 615 m water depth (station E). Sediment samples were obtained with a boxcorer, and the top layer of the sediment (0-0.5 cm) was collected with a spatula and immediately frozen at -20ºC.

3.3. Sample treatment and analytical procedures

Samples recovered from the sediment traps were stored in the dark at 2-4 ºC until they were processed in the laboratory with a modified version of the method described by Heussner et al. (1990). Large swimming organisms were removed by wet sieving through a 1 mm nylon mesh, while organisms <1mm were hand-picked under a microscope with fine-tweezers. Mineral grains >1 mm retained in the nylon mesh were also removed and considered as ice rafted detritus (see discussion section). Samples were split into 8 aliquots using a high precision peristaltic pump robot. One of the aliquots was immediately frozen at -20ºC for contaminant analyses. The other aliquots were repeatedly centrifuged to eliminate salt and formaldehyde, freeze-dried and weighed for total mass flux determination.

191 Total and organic carbon (OC) and total nitrogen (TN) contents, and the stable isotope
192 composition of OC, were measured on a Finnigan DeltaPlus XP mass spectrometer directly
193 interfaced to a FISONS NA2000 Element Analyzer via a Conflo interface for continuous flow
194 measurements at the Istituto di Scienze Marine (ISMAR-CNR). The results of isotopic analyses
195 are presented in the conventional δ notation. Samples for OC analysis were first treated with
196 HCl 1.5M to remove inorganic carbon (Nieuwenhuize et al., 1994). Although there is no
197 universal conversion factor to estimate organic matter from OC, in consistency with published
198 data nearby our study area we assumed organic matter as twice the OC content (Bauerfeind et
199 al., 2009). Carbonate content was calculated assuming all inorganic carbon is contained within
200 the calcium carbonate ($CaCO_3$) fraction using the molecular mass ratio 100/12.

201 Biogenic silica was analysed using a two-step extraction with 0.5 M Na_2CO_3 (2.5 h each)
202 separated after filtration of the leachate (Fabrés et al., 2002). Inductive Coupled Plasma Atomic
203 Emission Spectroscopy (ICP-AES) at the Scientific and Technological Centers of the University
204 of Barcelona was used to analyse Si and Al contents in the leachates, and a correction of the Si
205 of the first leachate by the Si/Al relation of the second leachate was applied to obtain the opaline
206 Si concentration (Kamatani and Oku, 2000). Corrected Si concentrations were transformed to
207 biogenic opal after multiplying by a factor of 2.4 (Mortlock and Froelich, 1989). The lithogenic
208 fraction was calculated assuming % lithogenic fraction = 100 - (%organic matter + %$CaCO_3$ +
209 %opal).

210 Grain size distribution was determined with a Coulter LS230 laser analyzer in samples with
211 enough material left after all major component analyses. A few grams of the freeze-dried
212 sample were oxidized with 10% H_2O_2, and then dispersed in approximately 20 cm^3 of water and
213 sodium polyphosphate and mechanically shaken for 4 h. Each sample was then introduced into
214 the particle size analyzer after using a 2 mm sieve to retain coarser particles that might obstruct
215 the flow circuit of the instrument. The measured particle size is presented as volume percentage
216 in a logarithmic scale.

217 Seabed sediment samples were freeze-dried, ground with an agate mortar and homogenized for
218 analyses. The same procedures as those for the sediment trap samples were applied.

219 **3.4. Confidence boundaries and sediment trap efficiency**

220 The coefficient of variation (CV) (ratio of the standard deviation to the mean) is a simple
221 standard measure of uncertainty. Total mass estimates and opal measurements had the largest
222 uncertainty, with a mean CV of 4.5% (Fabrés et al., 2002) and 4.1% (Heussner et al., 1990),
223 respectively. CV of replicate analysis of grain size was 2.2% (n=9), while those of OC and $\delta^{13}C$
224 show a CV of 1.7% (n=12) and 0.2% (n=7), respectively. Uncertainty bounds of major
225 components (lithogenic fraction, $CaCO_3$, organic carbon and opal) fluxes (propagated error
226 calculated as the quadratic sum of errors on mass and major component estimates) were always
227 lower than 6%.

228 These uncertainties indicate precision associated with laboratory and analytical procedures.
229 However, there are three other potential source of errors associated mainly to sediment trap
230 collection efficiencies which are 1) hydrodynamic bias, i.e. motion of the mooring line and its
231 impact on collecting sinking particles, 2) swimmers, or active migration of zooplankton into the
232 trap, and 3) solubilization or loss of material in the collecting cup (Buesseler et al., 2007). The
233 mooring lines deployed along the western margin of Spitsbergen were maintained taut by floats
234 mounted at the top of the line, and examination of current meter pressure sensors show that the
235 mooring line tilting was minimum even during strong current episodes (up to 36.3 cm s^{-1}). The
236 swimmer issue was solved through sieving and picking methods under a microscope. Those
237 intact animals appearing alive and thus though to have entered actively the sediment trap were
238 considered swimmers and removed from the sample to avoid a total mass flux bias. Finally, the
239 preservation issue was solved by adding formalin to preserve particle integrity and stop
240 continued bacterial breakdown of particles once collected. This poisoning solution appears to be
241 the most suitable compromise in terms of effectiveness and prevention of swimmer
242 fragmentation (Heussner et al., 1990; Buesseler et al., 2007; Lamborg et al., 2008).

243

4. Results

4.1. Sea ice and chl-a concentrations

The monthly maximum and minimum sea ice extent is illustrated in Fig. 2. Sea ice was absent from the western margin off Spitsbergen from July to November 2010 except for some land-fast ice in Storfjorden. Sea ice covered most of the SW part Spitsbergen from late December 2010 to early January 2011, including stations E, A and D. Later on, sea ice retreated towards the coast and disappeared around the Spitsbergen Island. Sea ice grew again in early April 2011 and reached stations E and A for a couple of days. By early May 2011, sea ice started to progressively melt, remaining only in the inner parts of Storfjorden until July 2011.

Temporal variations in the spatial distribution of chl-a concentration are illustrated in Fig. 3. Only data from April to September are shown as MODIS could not collect data during the months of darkness (October-March). Despite phytoplankton primary production is practically suppressed without irradiance (Boyd et al., 1995; Saggiomo et al. 2002), very low chl-a concentrations are observed in late winter months also in polar waters (Smith et al., 1991). The chl-a concentration increased over the mooring stations during late spring- summer months (April to August 2010 and 2011). Maximum concentrations exceeding 2.5 mg chl-a m^{-3} were recorded in May for both years, followed by decreasing concentration in the continental shelf and in the Spitsbergen fjords in June-July to values below 1 mg chl-a m^{-3}.

4.2. Time series of hydrographic conditions

At the study area, the current direction at 1000 m depth (station B) was highly variable (Fig. 4a), but the mean flow was clearly oriented along-slope toward the NW. Current speed measured at 1000 and 1500 m at station B showed similar fluctuations (Fig. 4b and c), but were slightly weaker at 1000 m depth (median of 7.4 ± 5.2 cm s^{-1}, maximum of 33.4 cm s^{-1}) than at 1500 m (median 9.5 ± 5.7 cm s^{-1}, maximum of 36.3 cm s^{-1}). The current variations were dominated by low frequency fluctuations of 2-8 days periodicity, and to a lesser extent by semi-diurnal tidal fluctuations. The currents showed a significant intensification during winter (from

mid-February to late March 2011, Fig. 4b). This seasonal variability is comparable to that recorded at the F4 (Fig. 4c) and F5 (Fig. 4d) sites further north in the Fram Strait. All records indicated a significant increase of the mean flow in March 2011 (monthly mean kinetic energy, Fig. 4e) together with larger high frequency current fluctuations from February to April 2011 (monthly eddy kinetic energy (EKE), Fig. 4f).

Low potential temperature ($\theta \sim -0.9$ °C) and salinity ($S \sim 34.91$) measured near the bottom at stations A and B (Fig. 5) are characteristic of the Norwegian Sea Deep Water (Hansen and Østerhus, 2000). The ephemeral increase in potential temperature ($\theta > 0$ °C) (at stations A and D) and salinity ($S > 34.92$) (at station A) observed in February 2011 around 1000 m (Fig. 5) suggests the remote influence of the shallower, warmer, and saltier Atlantic Water.

4.3. Total mass and major component fluxes

Vertical profiles of turbidity collected near the mooring sites on 23 July 2010 and 13 July 2011 showed the presence of a bottom turbid layer about 100-250 m thick at all stations (Fig. 6).

Temporal variations in total mass and major components (lithogenic fraction, $CaCO_3$, organic carbon and opal) fluxes are shown in Fig. 7, and in concentration of major components (as fraction of total mass) are shown in Fig. 8, respectively. Total mass fluxes at near bottom traps illustrated an arrival of particles in January, February and March 2011 especially at the shallowest and southernmost station A (maximum flux of 11646 mg m^{-2} d^{-1}) and decreasing northwards along the slope down to station C (maximum flux of 1073 mg m^{-2} d^{-1}). Particle fluxes then decreased at all stations but maintained relatively high levels until the end of the study period in July 2011. A small increase was recorded in June-July 2011 at the deeper stations B and C. In contrast, particle fluxes for the upper trap at mooring B (1000 m, 500 mab) were more or less one order of magnitude lower, and the highest fluxes were recorded in January 2011 (662 mg m^{-2} d^{-1}) and April 2011 (578 mg m^{-2} d^{-1}).

The flux of the major components followed the pattern of total mass fluxes with some variations. For the biogenic components at station A, fluxes peaked at 161 mg m^{-2} d^{-1} for OC,

(Fig. 7). At station A, OC and opal concentrations showed a clear seasonal pattern with low contents (<2.5% for OC and 1.5% for opal) from November to May and higher contents during the summer months (June-September, Fig. 8). The highest contents were found in the upper trap of station B with values of 10.4% and 6.7% of opal (Fig. 8). For the carbonated and lithogenic fractions, the highest fluxes were recorded in March 2011 at stations A and B near the seabed, in February 2011 at station D and in July at station C (Fig. 7). Concentrations of the lithogenic component, which ranged from 57 to 85%, were opposed to those of the biogenic components (OC and opal), with a summer minimum and a winter-spring maximum. Concentrations of $CaCO_3$ varied between 10 and 30% and roughly mirrored the variations of the lithogenic content (Fig. 8).

The stable isotope signature of settling OC ($\delta^{13}C$) varied between -23.1 and -25.5‰ (Fig. 8). Small variations were observed during the sampling period, with only sporadic depleted values found in January 2011 at station D, and in June 2011 at stations A, D, and B-Top. The maximum values were recorded during the spring period at all stations. In surface sediments, $\delta^{13}C$ ranged from -22.9‰ (recorded at the deepest station C, which also showed the highest OC content) and -24.3‰ (found at the shallowest station E, which also recorded the lowest OC content) (Table 1).

4.4. Grain size distribution of settling particles and surface sediments

Grain sizes of settling particles and surface sediments are shown in Fig. 9 (for sizes<1 mm) and Table 2 (for sizes>1 mm).

Settling particles collected from the sediment traps were predominantly composed of clay (<4 μm) and silt-sized (4-63 μm) particles, with sporadic contribution of sand-sized (>63 μm) particles in January 2011 at station D and March 2011 at station A (Fig. 9). Most of the samples showed the main modes at 4-8 and 20-26 μm (fine silt), while January and March 2011 samples showed modes at 26-40 μm (fine silt) and 56-76 μm (sand).

Very coarse fractions (mostly 2-4 mm particles but also fine gravel particles up to 8 mm) (Table 2) were observed at station D in January 2011. During this month, 207 grains with size larger than 1 mm were collected. The flux of those large particles, which has been excluded from total mass flux calculations, accounted however 414 grains m^2 $month^{-1}$ and 529 mg m^2 d^{-1} (about one fourth of the fine particle flux), and consisted of angular grains of detrital carbonate minerals with minor contributions of quartz, gneiss and shale grains (Fig. 10).

Surface sediments at stations B and C were mostly composed of silt sized particles, while sediments at stations E and D, which are those closer to the margin, showed high contents of very fine to medium gravel (Table 2). The main modes of fine grained particles were at 4-12 μm and 22-30 μm (stations A, B, C), 80-170 μm (stations E, A, D) and 400-780 μm (stations E, D) (Fig. 9).

5. Discussion

5.1. Main oceanographic conditions impacting downward particle fluxes

The barotropic character of the currents at station B along the slope is coherent with the summertime LADCP observation of Walczowski et al. (2005) on an E-W transect at the same latitude (76°30'N). They showed that the along-slope poleward flow was about 200 km wide and extended down to 2000 m depth with the shallow WSC core, which transports most of the AW, being restricted to the 800 m isobath. They also showed a strong barotropic component of the deep along-slope currents from the bottom to 500 m depth, with intensity between 5 and 15 cm s^{-1}, comparable to our observations (Fig. 4b). Based on current records between 1997 and 2010 in the Fram Strait (78°50'N), Beszczynska-Möller et al. (2013) showed that the narrow WSC core revealed no seasonal variability. The offshore branch of the WSC, on the other end, showed a strong seasonal variability with maximum in winter. During winter 2011, this winter maximum has been seen both at the study site and at the Fram Strait further north (Fig. 4e and f).

Downslope advection of dense, brine-enriched shelf waters overflowing from Storfjorden has not been identified from our data set. Although air temperatures did not reach the abnormally high temperatures recorded in winter 2011-2012 (Nordli et al., 2014), the winter 2010-2011 was also warmer than usual in Svalbard. Indeed, Arctic sea ice extent in February 2011 was one of the lowest ever recorded (Laxon et al., 2013), and Atlantic pelagic crustacean from temperate waters reproduced in the northern Fram Strait in summer 2011 (Kraft et al., 2013). These warm atmospheric conditions prevented massive ice production and salt rejection in Storfjorden in winter 2011 (Jardon et al., 2014), and thus water to gain enough density to cascade down the slope and propagate northwards into the Fram Strait (Fer et al., 2008). Furthermore, the winter intensification of the along-slope poleward flow may have affected sea ice extent through advection of heat, eddy stirring or double diffusive processes (Vinje, 2001; Saloranta and Haugan, 2004; Divine and Dick, 2006; Polyakov et al., 2012b), and may be responsible for the significant ice melt recorded in March 2011, when the ice edge shifted significantly towards the north and the east, and retreating from the northern fjords (Fig. 2).

During winter 2010-2011, intensification of deep currents (Fig. 4) seemed to have a major influence on the downward flux of particles. Given the description of the WSC structure and variability by Walczowski et al. (2005) and Beszczynska-Möller et al. (2013), it is likely that this intensification affected the different stations that span between depths of 1000 and 2000 m. Fine-grained sediments present at the outlet of the Storfjordrenna (Fig. 1) and the upper slope of the western Spitsbergen margin, initially deposited in the inner fjord and swept towards deeper areas during fall and winter months (Sternberg et al., 2001), were likely to be resuspended and transported northwards by the WSC (Fig. 4). Current amplitudes recorded were high enough to transport silt particles up to 33 μm as suspended load, as calculated by the Sedtrans05 sediment transport model of Neumeier et al. (2008), which corresponds to one of the main grain size modes for both surface sediments and settling particles (Fig. 9). In addition, settling particles during this event were relatively depleted in the OC and opal and resembled the composition of the surface sediments (Table 1). The diminution by one order of magnitude of the winter peak

of mass flux between 1000 m and 2000 m bottom depth suggests that the resuspension and/or bottom transport was particularly active at station A (1000 m) and in a lesser extent at station B (1500 m). The limitation of this transport to the bottom layer is confirmed by the absence of total mass flux increase in the trap moored at 500 m above the seabed (B-Top, Fig. 7). The presence of a bottom nepheloid layer at the different mooring sites between ~600 m (station E) and 2000 m depth (station C) suggests a relatively permanent presence of fine particles in suspension. Winkelmann and Knies (2005) inferred an active winnowing of fine sediments from outer continental shelf and upper slope sediments west of Spitsbergen.

Winter outbursts of lithogenic particle sedimentation reaching values of 83-950 mg m^{-2} d^{-1} were also found by Honjo et al. (1988) and Hebbeln (2000) in the eastern Fram Strait. They were related to lateral advection of dense water from the Barents Sea and ice rafted detritus (IRD) inputs, respectively. In both studies the sediment traps were placed at around 500 m above the seafloor, precluding any interception of resuspended particles from bottom sediments due to intensifications of the WSC. This is to our best knowledge the first study documenting active resuspension and transport in the bottom layer by the WSC of deep slope sediments.

The turbid layer and winnowing of fine sediment could be also triggered by other resuspension mechanisms, such as internal waves that produce elevated bed shear stress. Thorpe and White (1988) showed the occurrence of a strong intensification of the near bottom mixing and resuspension of sediments on the deep slope (2550 m) along the Porcupine Bank. This intensification was attributed to the critical reflection of the dominant M2 tidal wave when it has the same propagation slope as the seabed. Bonnin et al (2006) showed the potential of internal solitary waves in triggering near-bed mixing and resuspension of sediment at the foot of the slope of the Rockall Channel. Although hindered by the presence of ice and in average one to two order of magnitude less energetic than at lower latitudes (e.g. Levine et al., 1985; D'Asaro and Morison, 1992; Morozov and Paka; 2010; Guthrie et al., 2013), internal wave mixing might possibly lead to sediment resuspension and transport along the slope.

401 **5.2. Downward fluxes of iceberg rafted detritus and terrestrial organic matter**

402 Increased arrival of detrital carbonate mineral grains larger than 1 mm (mostly very fine gravel
403 but with contributions of medium gravel) at 1120 m depth (station D, Fig. 1) in January 2011
404 can be regarded as IRD. Ice rafting can occur by icebergs and sea ice that drift under the action
405 of ocean currents and melt releasing debris, falling to the seafloor. While icebergs released from
406 an ice sheet or glacier are more likely to transport large and angular particles such as those
407 caught by our sediment trap (Fig. 10), sea ice usually transports only fine-grained and more
408 rounded particles (Gilbert, 1990). However, this is not an unequivocal distinction between
409 iceberg and sea ice IRD. Indeed, large and angular particles eroded from coastal cliffs,
410 transported by rivers or even mobilized from the shelf seafloor can be entrained to land fast sea
411 ice (Darby et al., 2011). The fact that calving icebergs hardly reach the west coast of
412 Spitsbergen today (Müller and Knies, 2013), and that Storfjorden and most of the southwestern
413 Spitsbergen margin were completely covered by drifting sea ice during winter 2011 (Fig. 2),
414 suggest that those IRD were most likely sea ice-transported from the southern Spitsbergen
415 coast.

416 The $\delta^{13}C$ signature of OC allows to investigate the provenance of settling organic matter and
417 thus determine the importance of land derived material settling along with IRDs in January
418 2011. This approach takes advantage of the distinct signatures of the different types of organic
419 matter typically present in the continental margin (Hedges et al., 1998; Goñi et al., 1988).
420 Hence, terrestrial OC from C3 (carbon fixation via the Calvin-Benson cycle) plants in the Arctic
421 realm shows depleted $\delta^{13}C$ signatures around -26 to -28‰ (Goñi et al., 2000; Hop et al., 2006;
422 Winkelmann and Knies, 2005) (C4 (Hatch-Slack cycle) vegetation in the Arctic is
423 insignificant). In contrast, the $\delta^{13}C$ signature of marine OC in Arctic waters is more variable,
424 because slow growing phytoplankton under high concentration of dissolved CO_2 at low surface
425 water temperatures show depleted values (-20 to -26‰), while sea-ice algae growing under CO_2
426 limited conditions show highly enriched values (-15 to -18‰) (Schubert and Calvert, 2001;
427 Zhang et al., 2012). This variability in the marine signal of $\delta^{13}C$ leads to some uncertainty in the

use of $\delta^{13}C$ for identification of the organic matter sources. Investigating major trends in the provenance of organic matter (marine vs. terrigenous) we can assume that phytoplankton associated to warm, ice-free and relatively nutrient enriched surface waters from the WSC show a $\delta^{13}C$ value of -21‰, and that terrestrial derived organic matter show a $\delta^{13}C$ value of -27‰ (Schubert and Calvert, 2001; Winkelmann and Knies, 2005). Using a simple two end member isotopic mixing model to determine relative proportions of each source (Hedges et al., 1988; Goñi et al., 2000) we calculate that 75% of the downward flux of organic matter at station D in January 2011 was of terrestrial origin. Therefore, drifting sea ice contributed not only with large amounts of very fine to medium gravel but also with terrigenous organic matter. This is consistent with recent observations of high terrigenous organic carbon content in surface sediments below seasonally ice covered areas around southern Spitsbergen (Pathirana et al., 2014).

IRD and terrestrial organic matter were also present in surface sediments at stations E and D (Table 2). Progressively warming winter conditions in the last decades in the area (Walczowski and Piechura, 2007; Westbrook et al., 2009; Spielhagen et al., 2011; Ferré et al., 2012) may have resulted in melting sediment laden sea ice and deposition of land derived material offshore the western Spitsbergen continental margin at depths 500-1120 m. The winnowing of fine grains sediments by recurrent intensifications of the WSC may have left ice rafted boulders outstanding in the seafloor (Winkelmann and Knies, 2005).

These new data have important implications for paleoceanographic studies. Number of IRD per cm^2 of sediment, or number of IRD per gram of dry bulk sediment, is frequently used as a reliable tracer of sea ice and iceberg rafting. Indeed, anomalous occurrences of IRD layers have been documented during Heinrich events representing periodic collapses of the large ice sheets (Bond et al., 1992). The grain-size interval chosen to represent IRD has been variable, with higher grain sizes (>1 mm) near the continental margins and lower ranges (>150 μm) in open ocean settings (Hemming 2004, and references therein). Here we show that sea ice rafting from the southern Spitsbergen coast during present-day winter conditions is able to bring more than

414 IRD (higher than 1 mm) per m^2 to depths beyond 1000 m during 1 month. Rough calculation assuming one event of this magnitude per year suggests an IRD flux of 41 cm^{-2} ky^{-1}, in the higher ranges of those measured during the final deglaciation in Isfjorden (Forwick and Vorren, 2009).

5.3. Seasonality in primary production and carbon export to the deep seafloor

The first measurements of OC flux to the deep sea floor in the eastern Fram Strait took place in the mid-80s by Honjo et al. (1988), and have been repeatedly measured after that (Hebbeln, 2000; Thomsen et al., 2001). In addition, since 2000 the HAUSGARTEN observatory provides a unique long-term dataset of OC fluxes to the deep Fram Strait (Bauerfeind et al., 2009; Lalande et al., 2013). All authors have reported the typical seasonal cycle of high latitudes characterised by high percentages of the biogenic compounds (opal, OC and $CaCO_3$) in the downward fluxes linked to the phytoplankton bloom that usually takes place in May and is dominated by diatoms, increased sinking of fecal pellets during summer, and decreasing biogenic contribution towards dark winter months. Our data agrees with the seasonal cycle described above, and the high OC and opal concentrations recorded at the onset (August-September 2010) and the end (June-July 2011) of the sampling period reflect pelagic primary production in surface waters. Unfortunately, and because mooring deployment and recovery were performed during summer months, the analysis of the complete biological cycle has been interrupted and needs to be examined in the two different years.

Increased chl-a concentration is evident in the western Spitsbergen continental shelf in April 2011 (Fig. 3). This spring bloom may have developed due to increased solar radiation and ice-melt induced stratification, which lead to the CO_2 uptake by primary production of phytoplankton. The patch with high loadings of chl-a increased in May 2011, covered most of the eastern Fram Strait in June 2011, and started to vanish in July 2011.This corresponds well with the opal and OC concentrations of settling particles that started to increase in May and peaked in June-July 2011 (Fig. 6). OC and opal concentrations were well correlated (Pearson's correlation coefficient=0.87, n=59, $p<0.01$) which is consistent with a link between the

processes responsible for OC and opal delivery to the seafloor. This suggests that chl-a biomass and primary production were dominated by silica-secreting organisms such as diatoms (Hodal et al., 2012), therefore governing OC export in spring-summer in the eastern Fram Strait as found by Bauerfeind et al. (2009). Recent studies have reported a shift from dominance of diatoms to a dominance of small sized phytoplankton such as coccolithophores during anomalous "warm" years (Bauerfeind et al., 2009; Lalande et al., 2013), but our 1 year-round sediment trap experiment does not allow us to relate magnitude of biogenic fluxes to interannual anomalies or trends.

In addition, a tongue of water with very low chl-a concentration was evident in the coastal areas in June 2010 and 2011 (Fig. 3). This was probably caused by increased freshwater inputs from the island due to melting of snow and ice, which suppressed phytoplankton growth, when air temperatures began to rise consistently above zero (Cherkasheva et al., 2014). Together with the melting waters, sediments and inorganic particles may have been released (Beszczyeska-Møller et al. 1997). The depleted $\delta^{13}C$ values (around -24‰) of OC settling in June 2011 at all stations (Fig. 8) suggest that melt water discharge may have also transported terrestrial organic matter beyond the fjords and the Spitsbergen continental shelf, reaching the deep margin.

On an annual basis, time weighted fluxes of OC decreased progressively northwards from 22.1 g OC m^{-2} y^{-1} (station A), 11.8 g OC m^{-2} y^{-1} (station B), to 6.1 g OC m^{-2} y^{-1} (station C). Taking into account that primary production in surface waters should not be significantly different among stations (Fig. 4), the observed differences are consistent with decreased inputs of OC from the slope with increasing water depth. Annual OC fluxes in the trap at 525 mab at station B, which may reflect only vertical settling of particles with no influence from resuspension, show values of 4.7 g OC m^{-2} y^{-1}, similar to those obtained by Hebbeln (2000) and Honjo et al. (1988) in the same area. Using this level as a start point to parameterize the OC flux attenuation with depth of Martin et al. (1987) we obtain that the lateral input of OC in the lower water column at the 1500 m depth accounts for approximately 72% of the total downward flux. Most of this lateral flux is derived from the upper slope areas and has been advected during late

winter – early spring due to the reinforcement of the WSC (Fig. 4). Overall this indicates that the strength of the WSC is important not only for the organic carbon budget in the Arctic Ocean but also for the redistribution of carbon (i.e. food supply) to the deep sea fauna inhabiting the western Spitsbergen margin.

6. Conclusions and implications

Sedimentary dynamics in the continental margin west of Spitsbergen Island in 2010-2011 was influenced by three main natural drivers that were the northward flowing WSC, sea ice transport and the primary production of phytoplankton.

- An intensification of the currents was recorded in late winter – early spring 2011, that potentially resuspended and advected bottom sediments on the deep slope, mostly composed of lithogenic material with increased amounts of sand-sized particles. Grain size of both settling particles and surface sediments decreased with increasing water depth northwards, demonstrating the lowering capacity of the WSC to resuspend and transport sediment on the deep slope.
- Settling of IRDs played also a substantial role in sedimentary and carbon dynamics. Increased arrival of IRD larger than 1 mm was recorded in January 2011 and related to sea ice transport from the southern Spitsbergen coast. In addition, up to 75% of the settling OC during this event was derived from terrestrial sources. This highlights the importance of ice drifting from southern Spitsbergen not only as a source of IRD but also for the delivery of terrestrial organic matter the deep sediments of the eastern Fram Strait.
- Finally, primary production dominated by silica-secreting organisms was the main natural driver acting in late spring – summer. However, pelagic settling of OC represented less than 28% of the OC reaching the deep sea floor on an annual basis. Resuspension and lateral transport of OC from the upper slope areas due to reinforcement of the WSC likely represents the main source of OC buried in deeper areas of the Fram Strait, which has a

much better chance to enter the geological record and thus has a sustainable effect on carbon sequestration.

Our results show that particle fluxes and especially OC are strongly sensible to environmental conditions, highlighting that ongoing hydrographic changes in the Arctic Ocean will probably influence the distribution and cycling of OC, including shifting the relative magnitude of the main OC sources. Several studies suggest that reduced sea ice extent and thickness caused by global warming is likely to increase the export of marine organic matter as a result of a longer phytoplankton growing season (Wassman et al., 2006; Arrigo et al., 2008) and enhanced under-ice productivity (Boetius et al., 2013). Accordingly, coupled physical-biological models predict higher annual primary production rates and carbon export flux in the southern Spitsbergen shelves in coming decades, with significant impact on the food-limited and benthic environment that strongly depends on the delivery of organic matter from the water column (Reigstad et al., 2011). Furthermore, increases in river run-off and enhanced erosion of thawing permafrost in a warming climate may result also in increased delivery of terrestrial OC to the Spitsbergen shelves (Vonk et al., 2012). Climate driven changes in the intensity of the poleward WSC, which remain open to further confirmation, will determine where this organic material reaches higher depths and penetrate these anomalies into the deep Fram Strait ecosystems. While some studies predict an increase of the AW flow into the Arctic (Zhang et al., 1998; Karcher et al. 2003), other recent studies predict a decrease in the number of polar lows over the northeast Atlantic that would imply a potential weakening of the Atlantic meridional overturning circulation (Zhan and von Storch, 2010) and thus the intensity of the WSC (Skagseth et al., 2008). While increased WSC intensity would imply widely spreading of OC to the deep Fram Strait, decreased intensity would imply less advection and deposition of OC in the shelf and upper slope. To acquire a better understanding of all these processes, and assess the impact of climate change on them, further monitoring efforts in polar continental margins are needed, as is being performed for example in the nearby long-term open-ocean observatory HAUSGARTEN (Soltwedel et al., 2005).

Acknowledgements

This research has been supported by the projects HERMIONE (FP7-ENV-2008-1-226354) and GRACCIE-CONSOLIDER (CSD2007-00067), and a Catalan Government Grups de Recerca Consolidats grant (2009 SGR 1305). LL was partly supported by the CNR-DTA project SNOW (Sensor Network for Oceanography in shallow Water - Kongsfjord experiment), and AS by a "Ramon y Cajal" contract from MICINN. BF and JM are affiliated with the Centre of Excellence: Arctic Gas hydrate, Environment and Climate (CAGE) funded by the Norwegian Research Council (grant no. 223259). We are grateful to S. Buenz and the crew of RV Helmer Hansen (University of Tromsø) for their valuable support during the cruises, and R. Duran, S. Kunesch, J. Carbonne, A. Rumin, S. Aliani, and X. Rayo who assisted with the field and laboratory work. We also thank the three anonymous reviewers and J. Knies for their suggestions and comments. This is contribution N. XXXX of the CNR-ISMAR of Bologna.

576 **References**

577 Aagaard, K., Foldvik, A., Hillman, S.R., 1987. The West Spitsbergen Current: Disposition and
578 water mass transformation. Journal of Geophysical Research 92, 3778–3784.
579 Arrigo, K.R., Perovich D.K., Pickart, R.S., Brown, Z.W., van Dijken, G.L., Lowry, K.E., Mills,
580 M.M., Palmer, M.A., Balch, W.M., Bahr, F., Bates, N.R., Benitez-Nelson, C., Bowler, B.,
581 Brownlee, E., Ehn, J.K., Frey, K.E., Garley, R., Laney, S.R., Lubelczyk, L., Mathis, J.,
582 Matsuoka, A., Mitchell, B.G., Moore, G.W., Ortega-Retuerta, E., Pal, S., Polashenski,
583 C.M., Reynolds, R.A., Schieber, B., Sosik, H.M., Stephens, M., Swift, J.H,, 2012.
584 Massive phytoplankton blooms under Arctic sea ice. Science 336, 6087.
585 Bauerfeind, E., E., Nöthig, A. Beszczynska, K. Fahl, L. Kaleschke, K. Kreker, M. Klages, T.
586 Soltwedel, C. Lorenzen, J. Wegner, 2009. Particle sedimentation patterns in the eastern
587 Fram Strait during 2000–2005: Results from the Arctic long-term observatory
588 HAUSGARTEN. Deep Sea Research Part I 56, 1471-1487.
589 Beszczyeska-Møller, A., Weslawski, J. M., Walczowski, W. and Zajaczkowski, M., 1997:
590 Estimation of glacial meltwater discharge into Svalbard coastal waters. Oceanologia 39,
591 289-298.
592 Beszczynska-Möller, A.; Fahrbach, E., Rohardt, G., Schauer, U. (2012a): Physical
593 oceanography and current meter data from mooring F4-13. Alfred Wegener Institute,
594 Helmholtz Center for Polar and Marine Research, Bremerhaven,
595 doi:10.1594/PANGAEA.800353
596 Beszczynska-Möller, A., Fahrbach, E., Rohardt, G., Schauer, U. (2012b): Physical
597 oceanography and current meter data from mooring F5-13. Alfred Wegener Institute,
598 Helmholtz Center for Polar and Marine Research, Bremerhaven,
599 doi:10.1594/PANGAEA.800366
600 Beszczynska-Möller, A., Fahrbach, E., Schauer, U., Hansen, E., 2013. Variability in Atlantic
601 water temperature and transport at the entrance to the Arctic Ocean, 1997–2010. ICES
602 Journal of Marine Science. doi:10.1093/icesjms/fss056

603 Boetius A, Albrecht S, Bakker K, Bienhold C, Felden J, Fernández-Méndez M, Hendricks S,
604 Katlein C, Lalande C, Krumpen T, Nicolaus M, Peeken I, Rabe B, Rogacheva A, Rybakova
605 E, Somavilla R, Wenzhöfer F, et al., 2013. Export of Algal Biomass from the Melting Arctic
606 Sea Ice. Science 339: 1430-1432.
607 Bond G., Heinrich H., Broecker W. S., Labeyrie L., McManus J., Andrews J.T., Huon S.,
608 Jantschik R., Clasen S., Simet C., Tedesco K., Klas M., Bonani G., Ivy S., 1992.
609 Evidence for massive discharges of icebergs into the glacial Northern Atlantic. Nature
610 360, 245–249.
611 Bonnin J., Van Haren, H., Hosegood, P., Brummer, G.-J.A., 2006. Burst resuspension of seabed
612 material at the foot of the continental slope in the Rockall Channel. Marine Geology 226,
613 167–184
614 Boyd, P.W., S. Strom, F.A. Whitney, S. Doherty, M.E. Wen, P.J. Harrison, C.S. Wong, 1995.
615 The NE subarctic Pacific in winter: I. Biological standing stocks. Marine Ecology
616 Progress Series 128: 11-24.
617 Buesseler, K; Antia, A.; Chen, M.; Fowler, S.; Gardner, W.; Gustafsson, O.; Harada, K.;
618 Michaels, A.; Rutgers van der Loeff, M.; Sarin, M.; Steinberg, D.; Trull, T., 2007. An
619 assessment of the use of sediment traps for estimating upper ocean particle fluxes. Journal
620 of Marine Research 65, 345-416.
621 Carmack, E., and P. Wassmann. 2006. Food webs and physical-biological coupling on pan-
622 Arctic shelves: Comprehensive perspectives, unifying concepts and future research.
623 Progress in Oceanography 71, 446–477.
624 Carroll, M.L., and Carroll, J., 2003. The Arctic Seas. In K. Black and G. Shimmield eds.
625 Biogeochemistry of Marine Systems. Oxford Blackwell Pub Ltd. 127-156.
626 Cherkasheva, A., A. Bracher, C. Melsheimer, C. Köberle, R. Gerdes, E.-M. Nöthig, E.
627 Bauerfeind, A. Boetius, 2014. Influence of the physical environment on polar
628 phytoplankton blooms: A case study in the Fram Strait. Journal of Marine Systems 132,
629 196-207.

630 Comiso, J.C., C.L. Parkinson, R. Gersten, L. Stock, 2008. Acceleration decline in the Arctic Sea
631 ice cover. Geophysical Research Letters 35, L01703.
632 Darby, D., Myers, W., Jakobsson, M., Rigor, I., 2011. Modern dirty sea ice characteristics and
633 sources: The role of anchor ice. Jorunal of Geophysical Research 16, C09008.
634 D'Asaro, E.A., and Morison, J., 1992. Internal waves and mixing in the Arctic Ocean. Deep-Sea
635 Research 39, 459-484.
636 Divine, D., and Dick, C., 2006. Historical variability of sea ice edge position in the Nordic Seas.
637 Journal of Geophysical Research 111, 2156-2202.
638 Duarte, C.M., Agustí, S., Wassmann, P., Arrieta, J.M., Alcaraz, M., Coello, A., Marba, N.,
639 Hendriks, I.E., Holding, J., Garcia-Zarandona, I., Kritzberg, E., Vaqué, D., 2012. Tipping
640 Elements in the Arctic Marine Ecosystem. Ambio 4, 44–55
641 Elvevold, S., W. Dallmann, D. Blomeier., 2007. Geology of Svalbard. Norwegian Polar
642 Institute, Tromso. 36 pp.
643 Fabres, J., Calafat, A., Sanchez-Vidal, A., Canals, M., Heussner, S., 2002. Composition and
644 spatio-temporal variability of particle fluxes in the Western Alboran Gyre, Mediterranean
645 Sea. Journal of Marine Systems 33-34, 431-456.
646 Fer, I. and Ådlandsvik, B., 2008. Descent and mixing of the overflow plume from Storfjord in
647 Svalbard: an idealized numerical model study. Ocean Science 4, 115–132.
648 Ferré B., Mienert, J., Feseker, T. 2012. Ocean temperature variability for the past 60 years on
649 the Norwegian-Svalbard margin influences gas hydrate stability on human time scales.
650 Journal of Geophysical Research 117, C10017.
651 Forwick, M., and T.O. Vorren, 2009. Late Weichselian and Holocene sedimentary
652 environments and ice rafting in Isfjorden, Spitsbergen. Palaeogeography,
653 Palaeoclimatology, Palaeoecology 280, 258-274.
654 Gerland, S., Renner, A. H. H., Godtliebsen, F., Divine, D., and Løyning, T. B., 2008. Decrease
655 of sea ice thickness at Hopen, Barents Sea, during 1966–2007. Geophysical Research
656 Letters, 35, L06501.

Gilbert R., 1990. Rafting in glacimarine environments. In Glacimarine Environments: Processes and Sediments, Geological Society, London, Special Publication, eds Dowdeswell J.A., Scourse J.D. 53, pp 105–120.

Goñi, M.A., Ruttenberg, K.C., Eglinton, T.I., 1998. A reassessment of the sources and importance of land-derived organic matter in surface sediments from the Gulf of Mexico: Geochimica et Cosmochimica Acta 62, 3055–3075.

Goñi, M., M.B. Yunker, R.W. Macdonald, T.I. Eglinton, 2000. Distribution and sources of organic biomarkers in arctic sediments from the Mackenzie River and Beaufort Shelf. Marine Chemistry 71, 23-51.

Guthrie, J.D., Morison, J.H., Fer, I., 2013. Revisiting internal waves and mixing in the Arctic Ocean. Journal of Geophysical Research 118, 1-12

Hansen, B., and Østerhus, S., 2000. North Atlantic-Nordic Seas exchanges, Progress In Oceanography, 45(2), 109-208.

Hebbeln, D., 2000. Flux of ice-rafted detritus from sea ice in the Fram Strait. Deep-Sea Research Part II 47, 1773–1790

Hedges, J.I., Clark, W.A., Cowie, G.L., 1988. Organic matter sources to the water column and surficial sediments of a marine bay. Limnology and Oceanography 33, 1116-1136.

Hemming, S.R., 2004. Heinrich events: Massive Late Pleistocene detritus layers of the North Atlantic and their global climate imprint. Reviews of Geophysics 42, RG1005.

Heussner, S., Ratti, C., Carbonne, J., 1990. The PPS 3 timeseries sediment trap and the trap sample techniques used during the ECOMARGE experiment. Continental Shelf Research 10, 943–958

Hodal H., Falk-Petersen, S., Hop, H., Kristiansen, S., Reigstad, M., 2012. Spring bloom dynamics in Kongsfjorden, Svalbard: nutrients, phytoplankton, protozoans and primary production. Polar Biology 35, 191-203.

Honjo, S., S. J. Manganini, G. Wefer, 1988. Annual particle flux and a winter outburst of sedimentation in the northern Norwegian Sea. Deep-Sea Research 35, 1223-1234.

684 Hop, H., Falk-Petersen, S., Svendsen, H., Kwasniewski, S., Pavlov, V., Pavlova, O., Soreide, J.
685 E., 2006. Physical and biological characteristics of the pelagic system across Fram Strait
686 to Kongsfjorden. Prog. Oceanogr. 71, 182–231.
687 Intergovernmental Panel on Climate Change (IPCC) 2001: Climate change 2001: The Scientific
688 Basis. Contribution of Working Group I to the Third Assessment Report of the
689 Intergovernmental Panel on Climate Change, edited by J. J. McCarthy, O. F. Canziani, N.
690 A. Leary, D. J. Dokken and K. S. White (eds). Cambridge University Press, Cambridge,
691 United Kingdom and New York, USA.
692 Intergovernmental Panel on Climate Change (IPCC) 2007: Climate Change 2007: The Physical
693 Science Basis. Contribution of Working Group I to the Fourth Assessment Report of the
694 Intergovernmental Panel on Climate Change, edited by Solomon, S., D. Qin, M.
695 Manning, Z. Chen, M. Marquis, K.B. Averyt, M.Tignor and H.L. Miller. Cambridge
696 University Press, Cambridge, United Kingdom and New York, NY, USA.
697 Intergovernmental Panel on Climate Change (IPCC) 2013: Climate Change 2013: The Physical
698 Science Basis. Contribution of Working Group I to the Fifth Assessment Report of the
699 Intergovernmental Panel on Climate Change, edited by Stocker, T.F., D. Qin, G.-K.
700 Plattner, M. Tignor, S.K. Allen, J. Boschung, A. Nauels, Y. Xia, V. Bex and P.M.
701 Midgley. Cambridge University Press, Cambridge, United Kingdom and New York, NY,
702 USA.
703 Jakobsson, M., Mayer, L., Coakley, B., Dowdeswell, J. A., Forbes, S., Fridman, B., Hodnesdal,
704 H., Noormets, R., Pedersen, R., Rebesco, M., Schenke, H. W., Zarayskaya, Y., Accettella,
705 D., Armstrong, A., Anderson, R. M., Bienhoff, P., Camerlenghi, A., Church, I., Edwards,
706 M., Gardner, J. V., Hall, J. K., Hell, B., Hestvik, O., Kristoffersen, Y., Marcussen, C.,
707 Mohammad, R., Mosher, D., Nghiem, S. V., Pedrosa, M. T., Travaglini, P. G., and
708 Weatherall, P., 2012, The International Bathymetric Chart of the Arctic Ocean (IBCAO)
709 Version 3.0: Geophysical Research Letters 39, L12609.
710 Jardon, F. P., F. Vivier, P. Bouruet-Aubertot, A. Lourenço, Y. Cuypers, S. Willmes, 2014. Ice
711 production in Storfjorden (Svalbard) estimated from a model based on AMSR-E

observations: Impact on water mass properties. Journal of Geophysical Research 119, 377–393.

Kamatani, A., and Oku, O., 2000. Measuring biogenic silica in marine sediments. Marine Chemistry 68, 219-229.

Karcher, M. J., R. Gerdes, F. Kauker, C. Köberle, 2003. Arctic warming: Evolution and spreading of the 1990s warm event in the Nordic seas and the Arctic Ocean. Journal of Geophysical Research 108, 3034.

Kraft, A., Nöthig, E.M., Bauerfeind, E., Wildish, D.J., Pohle, G.W., Bathmann, U.V., Beszczynska-Möller, A., Klages, M., 2013. First evidence of reproductive success in a southern invader indicates possible community shifts among Arctic zooplankton. Marine Ecology Progress Series 493, 291-296.

Lalande, C., E. Bauerfeind, E. Nöthig, A. Beszczynska-Möller, 2013. Impact of a warm anomaly on export fluxes of biogenic matter in the eastern Fram Strait. Progress in Oceanography 109, 70-77.

Lamborg, C., Buesseler, K., Valdes, J., Bertrand, C., Bidigare, R., Manganini, S., Pike, S., Steinberg, D., Trull, T., Wilson, S., 2008. The flux of bio- and lithogenic material associated with sinking particles in the mesopelagic “twilight zone” of the northwest and North Central Pacific Ocean. Deep Sea Research Part II 55 (14-15), 1540-1563.

Laxon S. W., K. A. Giles, A. L. Ridout, D. J. Wingham, R. Willatt, R. Cullen, R. Kwok, A. Schweiger, J. Zhang, C. Haas, S. Hendricks, R. Krishfield, N. Kurtz, S. Farrell, M. Davidson, 2013. CryoSat-2 estimates of Arctic sea ice thickness and volume. Geophysical Research Letters 40, 732–737.

Levine, M. D., Paulson, C. A., Morison, J. H., 1985. Internal waves in the Arctic Ocean: observations and comparison with lower latitude climatology. Journal of Physical Oceanography 15, 800–809.

Loeng, H., 1991. Features of the physical oceanographic conditions of the Barents Sea. Polar Research, 10, 5-18.

739 MacGilchrist, G.A., A.C. Naveira Garabato, T. Tsubouchi, S. Bacon, S. Torres-Valdés, K.
740 Azetsu-Scott, 2014. The Arctic Ocean carbon sink. Deep Sea Research Part I 86, 39-55.
741 Manley, T.O., 1995. Branching of Atlantic Water within the Greenland-Spitsbergen Passage:
742 An estimate of recirculation. Journal of Geophysical Research 100, 20627–20634.
743 Martin, J.H., Knauer, G., Karl, D.M., Broenkow, W.W., 1987. VERTEX: carbon cycling in the
744 northeast Pacific. Deep-Sea Research 34, 267-285.
745 McClain, C.R., A.P. Allen, D.P. Tittensor, M.A. Rex, 2012. Energetics of life on the deep
746 seafloor. Proceedings of the National Academy of Sciences 109, 15366-15371.
747 Morozov, E.G., and Paka, V.T., 2010. Internal waves in a high-latitude region. Oceanology 50,
748 668–674
749 Mortlock, R.A., and Froelich, P.N., 1989. A simple method for the rapid determination of
750 biogenic opal in pelagic marine sediments. Deep-Sea Research 36, 1415– 1426
751 Müller, A. and Knies, J., 2013. Trace elements and cathodoluminescence of detrital quartz in
752 Arctic marine sediments – a new ice-rafted debris provenance proxy. Climates of the Past
753 9, 2615-2630.
754 Neumeier U., Ferrarin C., Amos C.L., Umgiesser G., Li M.Z., 2008. Sedtrans05: An improved
755 sediment-transport model for continental shelves and coastal waters with a new algorithm
756 for cohesive sediments. Computer & Geosciences 34, 1223-1242.
757 Nieuwenhuize, J., Maas, Y.E.M., Middelburg, J.J., 1994. Rapid analysis of organic carbon and
758 nitrogen in particulate materials. Mar. Chem. 45, 217– 224
759 Nilsen, F., F. Cottier, R. Skogseth, S. Mattsson, 2008. Fjord–shelf exchanges controlled by ice
760 and brine production: The interannual variation of Atlantic Water in Isfjorden, Svalbard.
761 Continental Shelf Research 28, 1838-1853.
762 Nordil, Ø., Przybylak, R., Ogilvie, A.E.J., Isaksen, K., 2014. Long-term temperature trends and
763 variability on Spitsbergen: the extended Svalbard Airport temperature series, 1898-2012.
764 Polar Research 33, 21349.

765 Owrid, G., Socal, G., Civitarese, G., Luchetta, A., Wiktor, J., Nöthig, E., Andreassen, I.,
766 Schauer, U., Strass, V., 2000. Spatial variability of phytoplankton, nutrients and new
767 production estimates in the waters around Svalbard. Polar Research 19, 155-171.
768 Parkinson, C. L., D. J. Cavalieri, P. Gloersen, H. J. Zwally, J. C. Comiso, 1999. Arctic sea ice
769 extents, areas, and trends, 1978-1996. Journal of Geophysical Research 104, 20837-
770 20856.
771 Pathirana, I., Knies, J., Felix, M., Mann, U., 2014. Towards an improved organic carbon budget
772 for the western Barents Sea shelf. Climates of the Past, 10, 569-587.
773 Polyakov, I.V., J. E. Walsh, R. Kwok, 2012a. Recent changes of arctic multiyear sea iIce
774 coverage and the likely causes. Bulletin of the American Meteorological Society, 93,
775 145–151.
776 Polyakov, I.V., A.V. Pnyushkov, R. Rember, V.V. Ivanov, Y.-D. Lenn, L. Padman, E.C.
777 Carmack, 2012b. Mooring-Based Observations of Double-Diffusive Staircases over the
778 Laptev Sea Slope. Journal of Physical Oceanography 42, 95–109.
779 Quadfasel, D., J.-C. Gascard, and K.-P. Koltermann, 1987. Large-scale oceanography in Fram
780 Strait during the 1984 Marginal Ice Zone Experiment. Journal of Geophysical Research
781 92, 6719–6728.
782 Reigstad, M., Carroll, J., Slagstad, D., Ellingsen, I., Wassmann, P., 2011. Intra-regional
783 comparison of productivity, carbon flux and ecosystem composition within the northern
784 Barents Sea. Progress in Oceanography 90 (1–4), 33-46.
785 Richardson, K., Markager, S., Buch, E., Lassen, M.F., Kristensen, A.S., 2005. Seasonal
786 distribution of primary production, phytoplankton biomass and size distribution in the
787 Greenland Sea. Deep Sea Research I 52, 979-999.
788 Saggiomo V., Catalano G., Mangoni O., Budillon G., Carrada G.C., 2002. Primary production
789 processes in ice-free waters of the Ross Sea (Antarctica) during the austral summer 1996.
790 Deep-Sea Research Part II 49: 1787-1801.
791 Saloranta, T.M., and Haugan, P.M., 2004. Northward cooling and freshening of the warm core
792 of the West Spitsbergen Current. Polar Research 23, 79-88.

793 Schubert, C.J., and Calvert, S.E., 2001. Nitrogen and carbon isotopic composition of marine and
794 terrestrial organic matter in Arctic Ocean sediments: implications for nutrient utilization
795 and organic matter composition. Deep Sea Research I 48, 789-810.
796 Schlichtholz, P. and Houssais, M.-N., 2002. An overview of the theta - S correlations in Fram
797 Strait based on the MIZEX 84 data. Oceanologia 44, 243-272.
798 Skogseth, R., P.M. Haugan, J. Haarpaintner, 2004. Ice and brine production in Storfjorden from
799 four winters of satellite and in situ observations and modelling. Journal of Geophysical
800 Research 109, C10008.
801 Skagseth, Ø., Furevik, T., Ingvaldsen, R., Loeng, H., Mork, K.A., Orvik, K. A.,Ozhigin, V.,
802 2008. Volume and heat transports to the Arctic Ocean via the Norwegian and Barents
803 Seas, in: Dickson, R., Meincke, J., Rhines, P. (Eds), Arctic Subarctic Ocean Fluxes:
804 Defining the Role of the Northern Seas in Climate. Springer, New York, pp. 45-64.
805 Smith Jr. W.O., Brightman R.I., Booth B.C., 1991. Phytoplankton biomass and photosynthetic
806 response during the winter-spring transition in the Fram Strait. Journal of Geophysical
807 Research: Oceans 96 (C3): 4549–4554
808 Smith K.L., B. H. Robison, J. J. Helly, R. S. Kaufmann, H. A. Ruhl, T. J. Shaw, B. S. Twining,
809 M. Vernet, 2007. Free-Drifting Icebergs: Hot Spots of Chemical and Biological
810 Enrichment in the Weddell Sea. Science 317, 478-482.
811 Soltwedel T., Bauerfeind E., Bergmann M., Budaeva N., Hoste E., Jaeckisch N., von Juterzenka
812 K., Matthiessen J., Mokievsky V., Nöthig E.-M., Quéric N.-V., Sablotny B., Sauter E.,
813 Schewe I., Urban-Malinga B., Wegner J., Wlodarska-Kowalczuk M., Klages M., 2005.
814 HAUSGARTEN: Multidisciplinary Investigations at a Deep-Sea, Long-Term Observatory in
815 the Arctic Ocean. Oceanography 18 (3):46–61.
816 Spielhagen, R.F., K. Werner, S. Aagaard Sørensen, K. Zamelczyk, E. Kandiano, G. Budeus, K.
817 Husum, T. M. Marchitto, M. Hald, 2011. Enhanced Modern Heat Transfer to the Arctic
818 by Warm Atlantic Water. Science 331, 450-453
819 Spreen, G., L. Kaleschke, G. Heygster, 2008. Sea ice remote sensing using AMSR-E 89 GHz
820 channels. Journal of Geophysical Research 113, C02S03.

821 Sternberg, R.W., Aagaard, Cacchione, D., Wheatcroft, R.A., Beach, R.A., Roach, A.T.,
822 Marsdeng, M.A.H., 2001. Long-term near-bed observations of velocity and hydrographic
823 properties in the northwest Barents Sea with implications for sediment transport.
824 Continental Shelf Research 21, 509-529.
825 Thomsen, C., Blaume, F., Fohrmann, H., Peeken, Ilka, Zeller, U., 2001. Particle transport
826 processes at slope environments - event driven flux across the Barents Sea continental
827 margin. Marine Geology, 175, 237-250.
828 Thorpe, S.A., and White, M., 1988. A deep intermediate nepheloid layer. Deep Sea Research 35
829 (9), 1665-1671.
830 Vinje, T., 2001. Anomalies and trends of sea ice extent and atmospheric circulation in the
831 Nordic Seas during the period 1864-1998. Journal of Climate 14, 255-267.
832 Wadhams P., 2013. Diminishing Sea-Ice Extent and Thickness in the Arctic Ocean. NATO
833 Science for Peace and Security Series C: Environmental Security 135: 15-30.
834 Walczowski, W., and Piechura J., 2007. Pathways of the Greenland Sea warming. Geophysical
835 Research Letters 34, L10608.
836 Walczowski, W., Piechura, Osinski, R., Wieczorek, P., 2005. The West Spitsbergen Current
837 volume and heat transport from synoptic observations in summer. Deep-Sea Research I,
838 52, 1374-1391
839 Wang M.Y., Overland J. E., 2009. A sea ice free summer Arctic within 30 years? Geophysical
840 Research Letters 36, L07502.
841 Wassmann, P., Reigstad, M., Haug, T., Rudels, B., Carroll, M. L., Hop, H., Gabrielsen, G. W.,
842 Falk-Petersen, S., Denisenko, S. G., Arashkevich, E., Slagstad, D., Pavlova, O., 2006.
843 Food webs and carbon flux in the Barents Sea. Progress in Oceanography 71, 232–287.
844 Wassmann, P., C.M. Duarte, S. Agusti, M. Sejr. 2011. Footprints of climate change in the
845 Arctic marine ecosystem. Biological Global Change 17, 1235-1429.
846 Westbrook, G. K., et al., 2009. Escape of methane gas from the seabed along the West
847 Spitsbergen continental margin. Geophysical Research Letters 36, L15608.

Whiteman, G., Hope, C., and Wadhams, P., 2013. Climate science: Vast costs of Arctic change. Nature 499, 401-403.

Winkelmann, D., and Knies, J., 2005. Recent distribution and accumulation of organic carbon on the continental margin west off Spitsbergen. Geochemistry, Geophysics, Geosystems 6, Q09012.

Zahn, M., and von Storch, H., 2010. Decreased frequency of North Atlantic polar lows associated with future climate warming. Nature 467, 309–312.

Zhang, J., A. Rothrock, and M. Steele, 1998. Warming of the Arctic Ocean by a strengthened Atlantic inflow: model results. Geophys. Res. Lett. 25, 1745-1748.

Zhang, R., M. Chen, L. Guo, Z. Gao, Q. Ma, J. Cao, Y. Qiu, Y. Li, 2012. Variations in the isotopic composition of particulate organic carbon and their relation with carbon dynamics in the western Arctic Ocean. Deep Sea Research Part II 81-84, 72-78.

861 **Figure captions**

862 **Figure 1.** Maps of the study area and station location. a) Main currents in the study area: red
863 arrows show the warm Atlantic Water within the West Spitsbergen Current (WSC), blue arrows
864 show the cold East Greenland Current (EGC) and the Eastern Spitsbergen Current (ESC), and
865 black arrow show the overflow plume from Storfjorden (Brine enriched Shelf Water, BSW).
866 Location of the moored stations F4 and F5 by Beszczynska-Möller et al. (2012a,b) is also
867 shown. b) Bathymetric map of the study area in the western margin off Spitsbergen with the
868 location of the moored stations A (1040 m), B (1500 m), C (2011 m), and D (1120 m), and the
869 extra-station E (615 m). Bathymetric data from IBCAO 3.0 (Jakobsson et al., 2012).

870 **Figure 2.** Maximum (red line, marks 95% ice-concentration isoline) and minimum (blue line,
871 marks 30% ice-concentration isoline) ice extent and day of the month recorded (number). The
872 location of the moored stations are also shown. The shaded area results from the different
873 projection of the obtained sea ice data and the projection used in all figures.

874 **Figure 3**. Chlorophyll-a concentration (mg m^{-3}) during spring-summer months of 2010 and
875 2011 when sunlight allowed MODIS measurements. Locations of moored stations are also
876 shown.

877 **Figure 4.** Times series recorded at station B from 23 July 2010 to 13 July 2011. a) Stick plot of
878 the current at 1000 m depth at station B, the inset shows the major and minor axes of the current
879 ellipse (in black) and the mean current (in red); b) times series of current speed at 1000 m and
880 1500 m at station B; c) times series of current speed at 750 m and 1410 m at station F4; d) times
881 series of current speed at 750 m, 1500 m, and 2130 m at station F5; e) time series of mean
882 kinetic energy (MKE=($\langle u \rangle^2 + \langle v \rangle^2$)/2), and (f) eddy kinetic energy (EKE= ($\sigma_u + \sigma_v$)/2) of the
883 currents. Energies are estimated using a moving window of 1 month; $\langle u \rangle$ and $\langle v \rangle$ are the
884 average longitudinal and latitudinal components of the current, and σ_u^2 and σ_v^2 are the variance
885 of the longitudinal and latitudinal components of the current.

886 **Figure 5**. θ-S diagrams from the near-bottom temperature–salinity records from 23 July 2010 to
887 13 July 2011 at station A at 1000 m (red) and station B at 1500 m (blue). Values with $\theta > 0°C$
888 and $S > 34.92$, characteristics of Atlantic Water, mainly appeared during February 2011.

889 **Figure 6**. Profiles of turbidity (Formazin Turbidity Unit, FTU) collected next to the mooring
890 sites on 23 July 2010 (solid line) and 13 July 2011 (dotted line).

891 **Figure 7**. Time series of total mass flux (TMF, mg m^{-2} d^{-1}) and major component fluxes
892 (lithogenic fraction, $CaCO_3$, organic carbon (OC) and opal, logarithmic scale, mg m^{-2} d^{-1}) at the
893 four near-bottom traps (25 mab) at stations A (~1000 m), D (~1120 m), B (1500 m) and C
894 (~2000 m), and B-Top (1000 m).

895 **Figure 8**. Time series of concentration of major components (lithogenic fraction, $CaCO_3$,
896 organic carbon (OC) and opal, %) and $\delta^{13}C$ (‰) values at the four near-bottom traps (25 mab) at
897 stations A (~1000 m), D (~1120 m), B (1500 m) and C (~2000 m), and B-Top (1000 m).

898 **Figure 9.** Grain size distribution of the fraction <1 mm of a) surface (0-0.5 cm) sediments, and
899 b) settling particles in October 2010 (shaded area) and January 2010 (station D) or March 2011
900 (stations A, B and C) (black line). Vertical lines show clay (<4 μm), silt (4-63 μm) and sand
901 (>63 μm) sizes.

902 **Figure 10.** Photograph of the ice rafted debris (IRD) collected at station D in January 2011
903 separated by coarse sand (1-2 mm), very fine gravel (2-4 mm), and fine gravel (4-8 mm).

904

905 **Tables**

906

907 **Table 1.** Organic carbon content (OC, wt.%), biogenic opal (opal, wt.%), calcium carbonate
908 ($CaCO_3$, wt.%), and lithogenic fraction (litho., wt.%) and the stable isotope of OC ($\delta^{13}C$, ‰) of
909 surface (0-0.5 cm) sediments at all stations. *bdl*: below detection limit.

910

	Depth (m)	OC (%)	opal (%)	$CaCO_3$ (%)	Litho. (%)	$\delta^{13}C$ (‰)
Station E	615	0.84%	*bdl*	9.12%	89.21%	-24.3
Station A	1000	0.90%	*bdl*	13.29%	84.90%	-23.2
Station D	1120	0.89%	*bdl*	6.55%	91.66%	-24.1
Station B	1500	1.12%	0.28%	14.37%	83.11%	-22.7
Station C	2000	1.13%	0.28%	14.39%	83.07%	-22.9

911

912

913 **Table 2.** Grain sizes (vol.%) of settling particles in January 2011 at station D and surface
914 sediments at stations E (615 m) to C (2000 m), including particles >1 mm. Particle sizes are
915 classified as clay (<4 μm), silt (4-63 μm), sand (63-1000 μm), coarse sand (1-2 mm), very fine
916 gravel (2-4 mm), fine gravel (4-8 mm), and medium gravel (8-16 mm). Particles >1 mm have
917 been considered IRD in the text.

918

	Depth (m)	Clay (%)	Silt (%)	Sand (%)	Coarse sand (%)	Very fine gravel (%)	Fine gravel (%)	Medium gravel (%)
Settling particles								
Station D	1120	4.69	11.21	1.26	4.04	43.73	35.05	0
Surface sediments								
Station E	615	9.36	21.63	29.31	0	9.02	19.71	10.96
Station A	1000	19.49	47.05	33.46	0	0	0	0
Station D	1120	7.09	14.21	22.29	0	11.95	18.16	26.30
Station B	1500	19.81	67.27	12.30	0	0.62	0	0
Station C	2000	23.31	69.25	7.44	0	0	0	0

919

Figure 1

Click here to download Figure: FIGURE 1.pdf

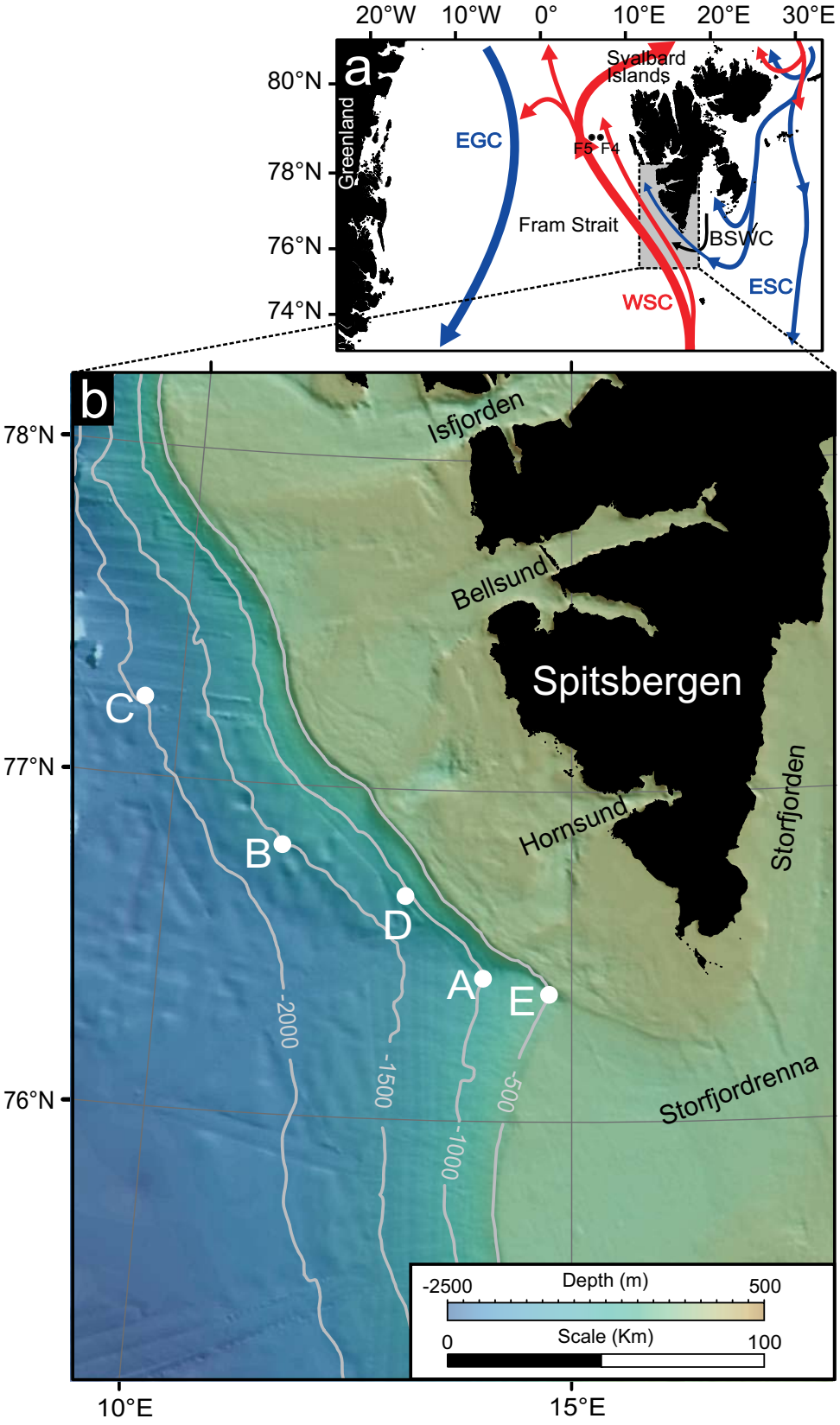

Figure 2

Click here to download Figure: FIGURE 2.pdf

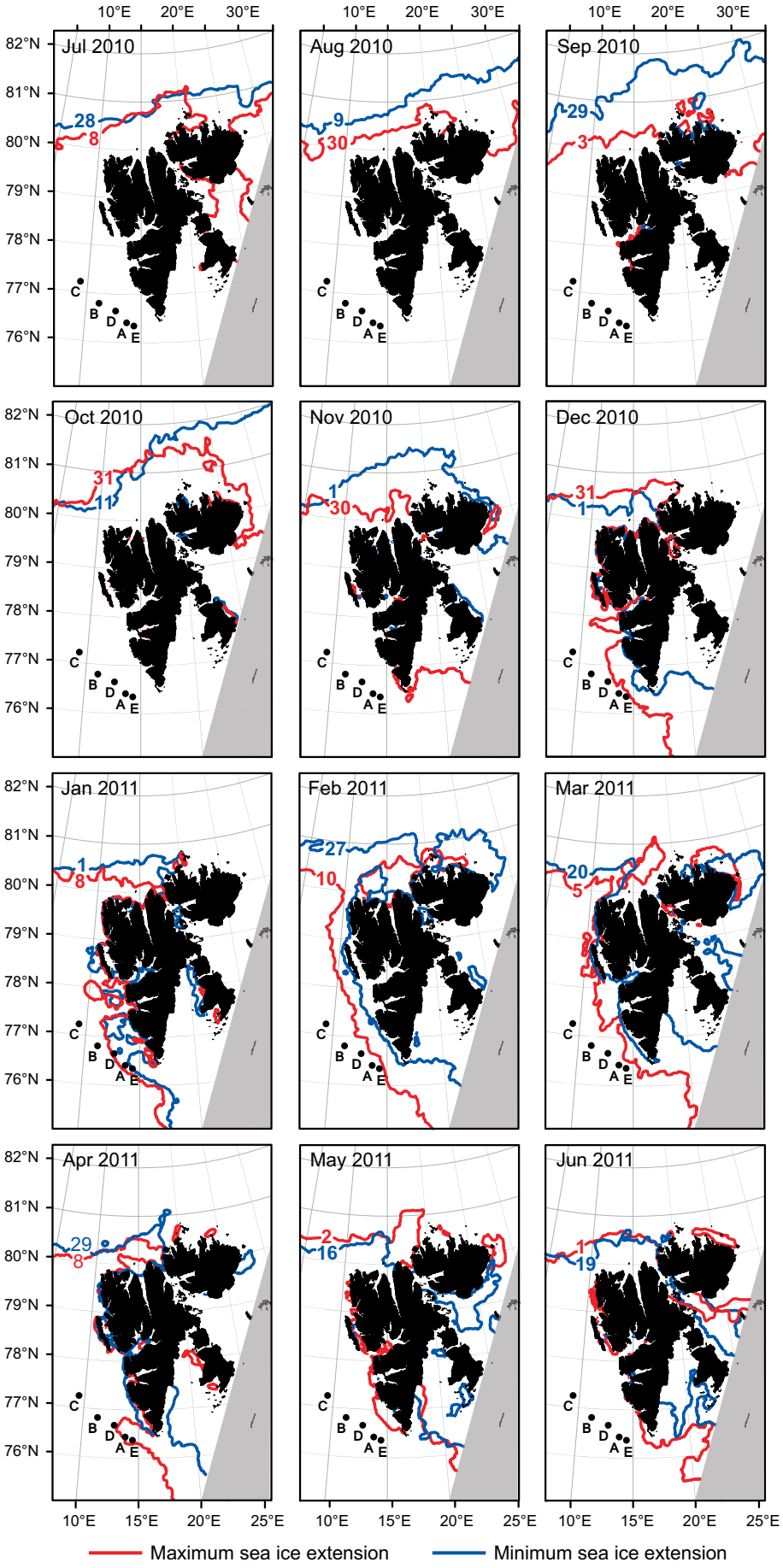

Figure 3

Click here to download Figure: FIGURE 3.pdf

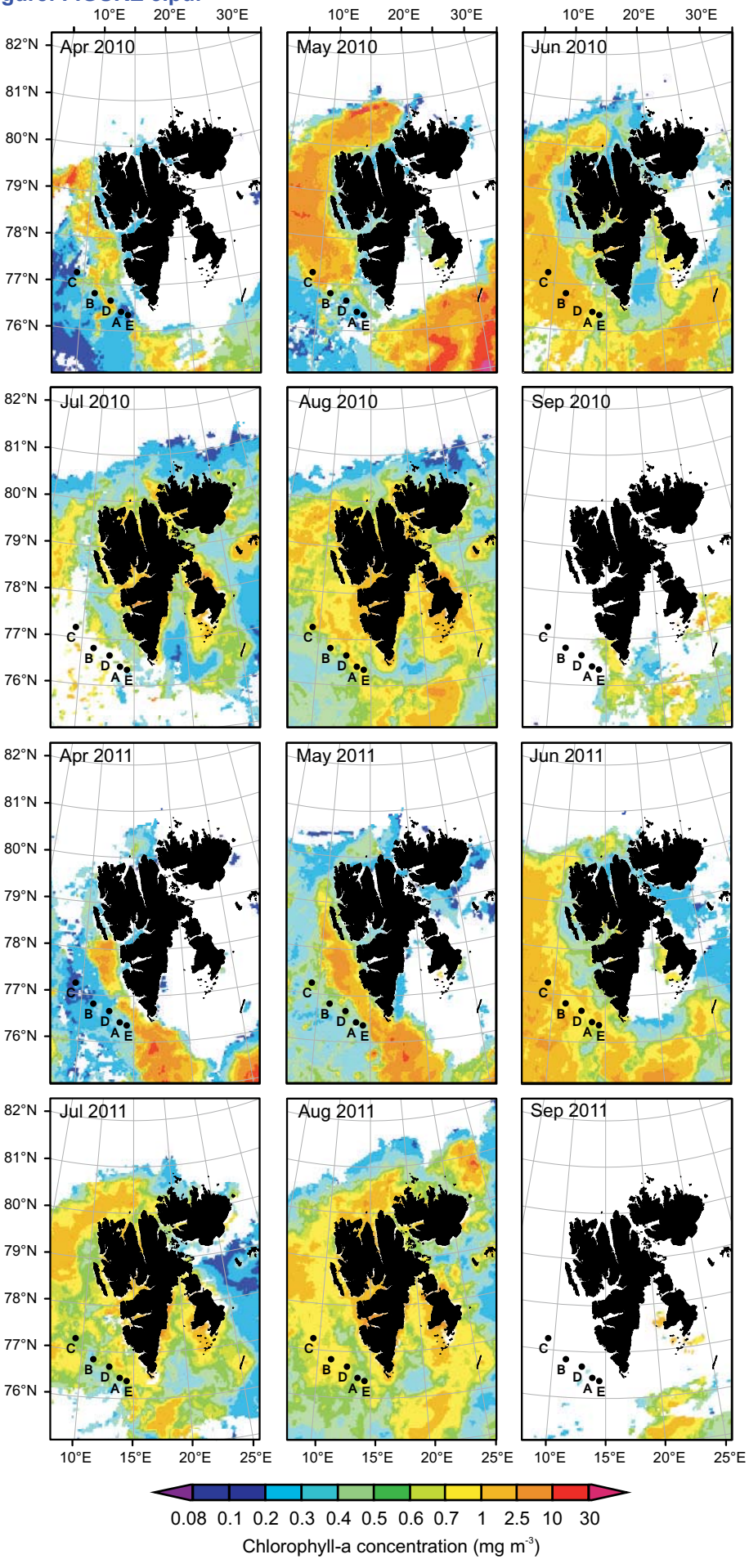

Figure 4

Click here to download Figure: FIGURE 4.pdf

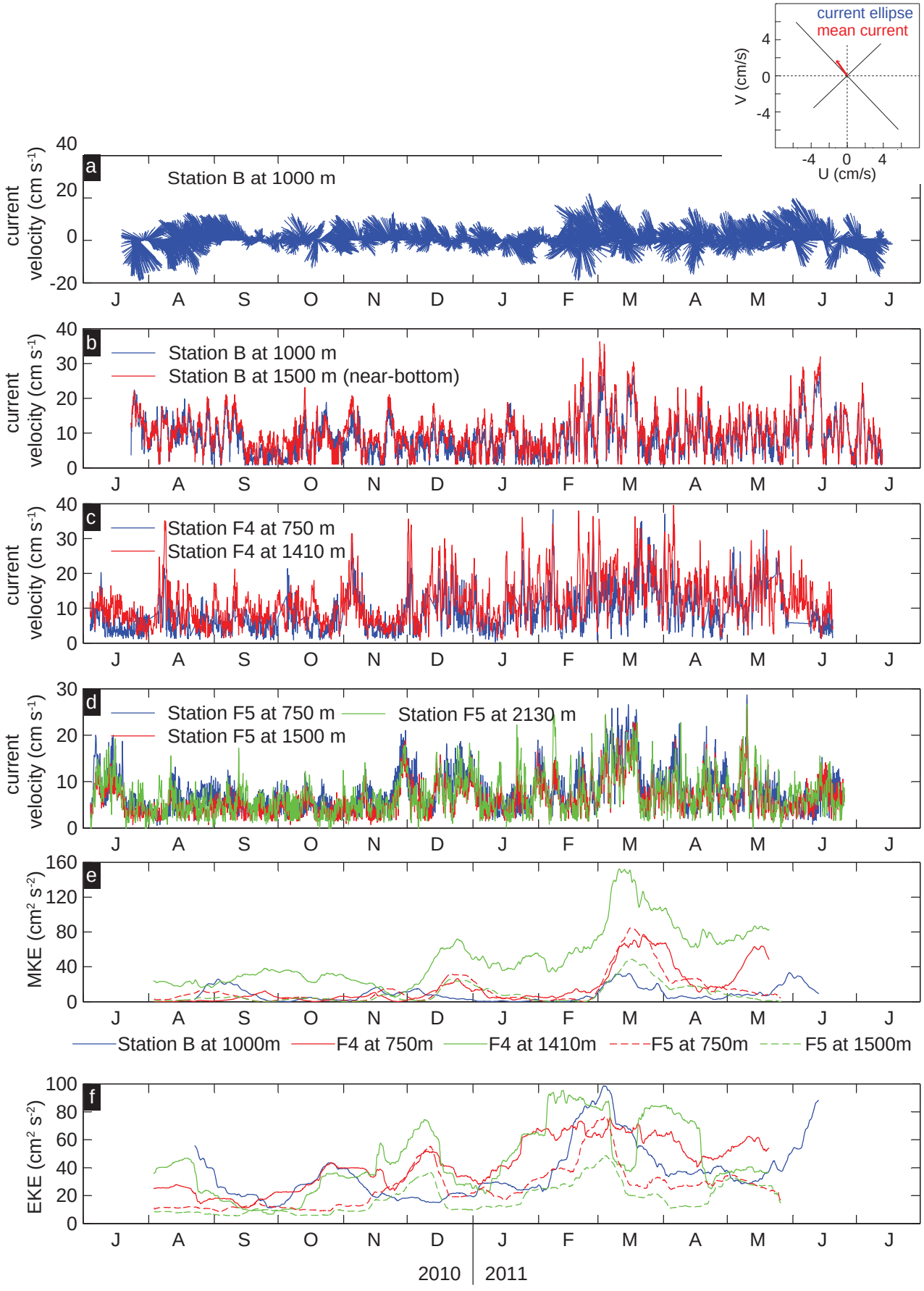

Figure 5

Click here to download Figure: FIGURE 5.pdf

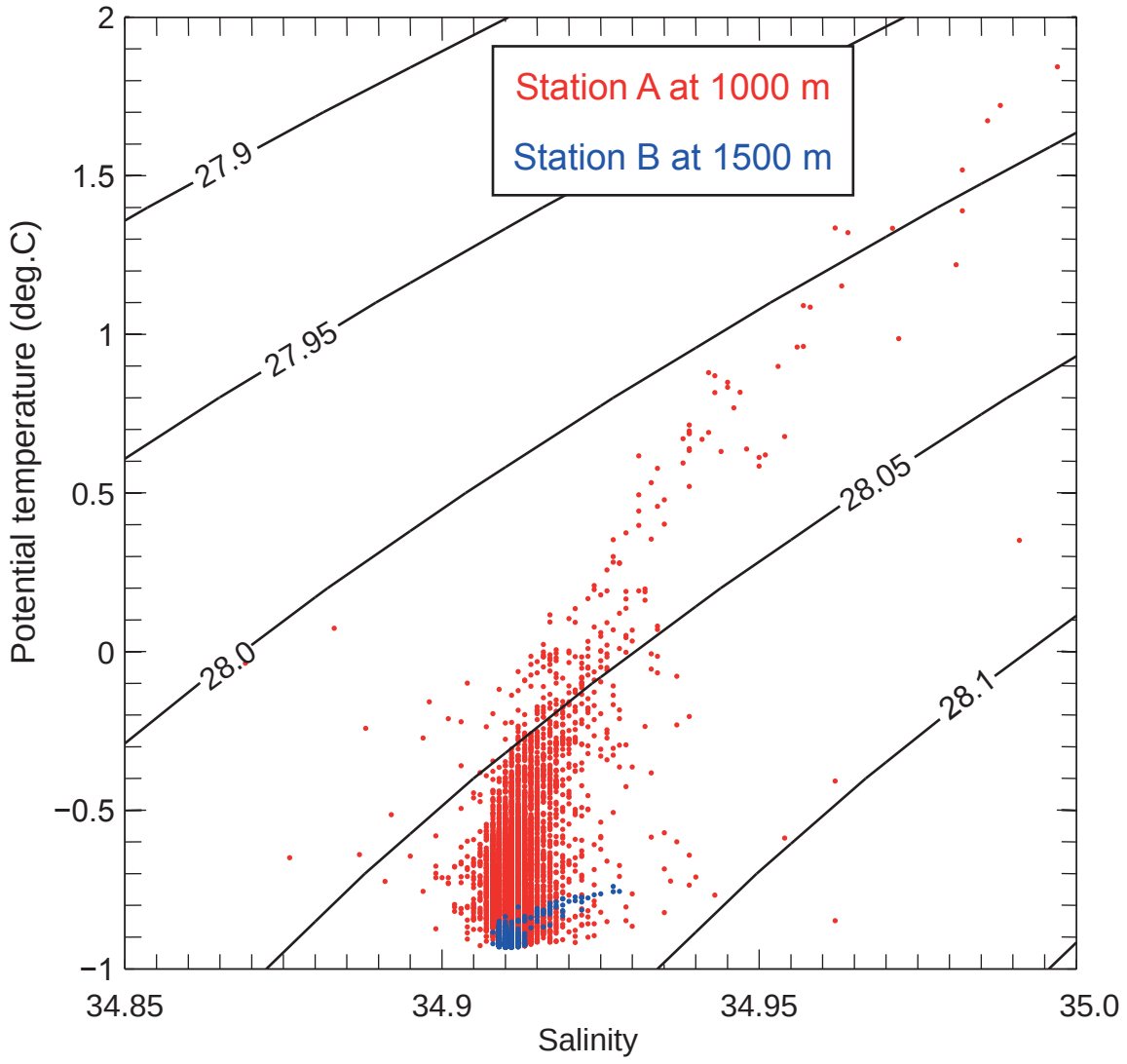

Figure 6
Click here to download Figure: FIGURE 6.pdf

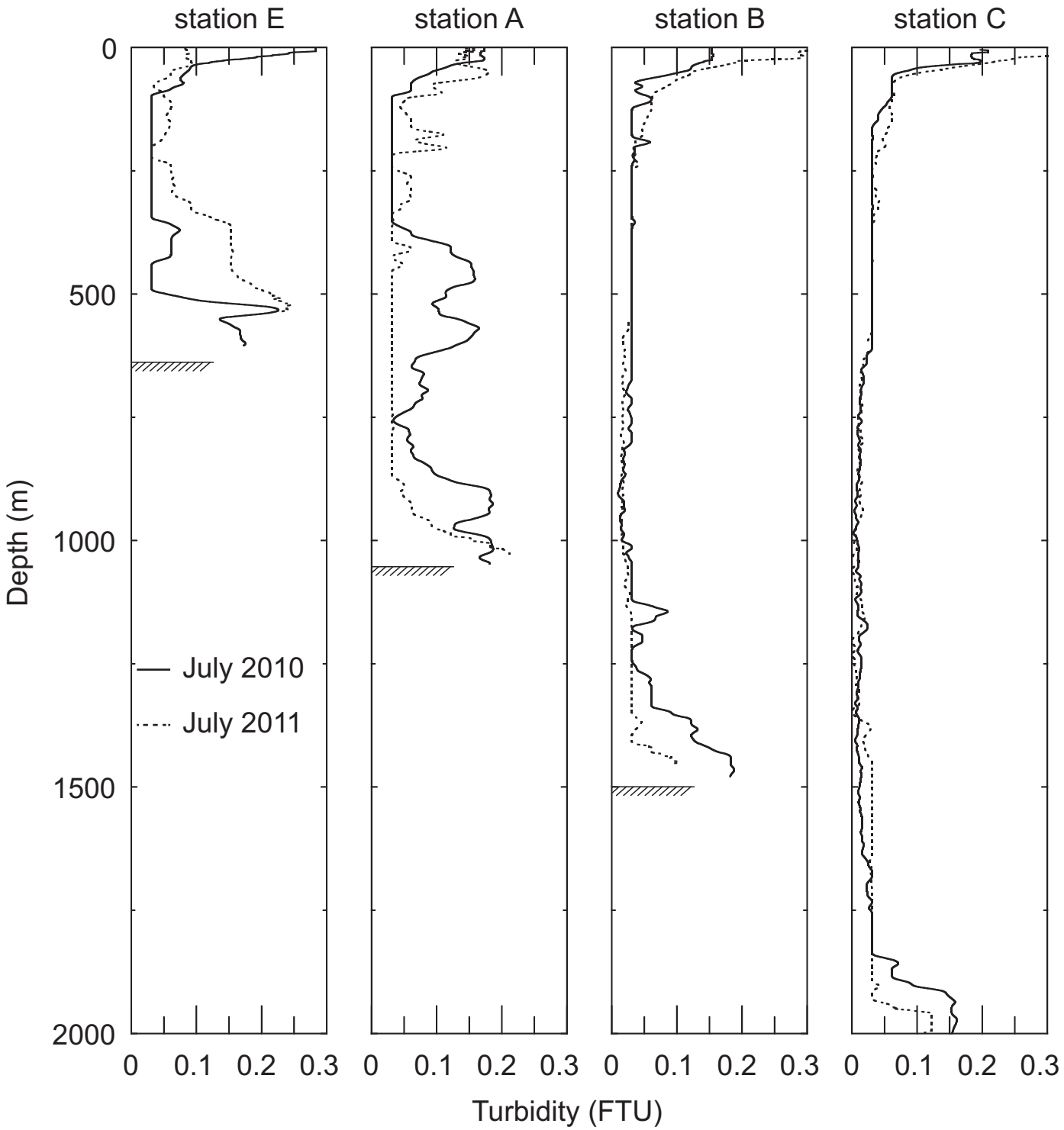

Figure 7

Click here to download Figure: FIGURE 7.pdf

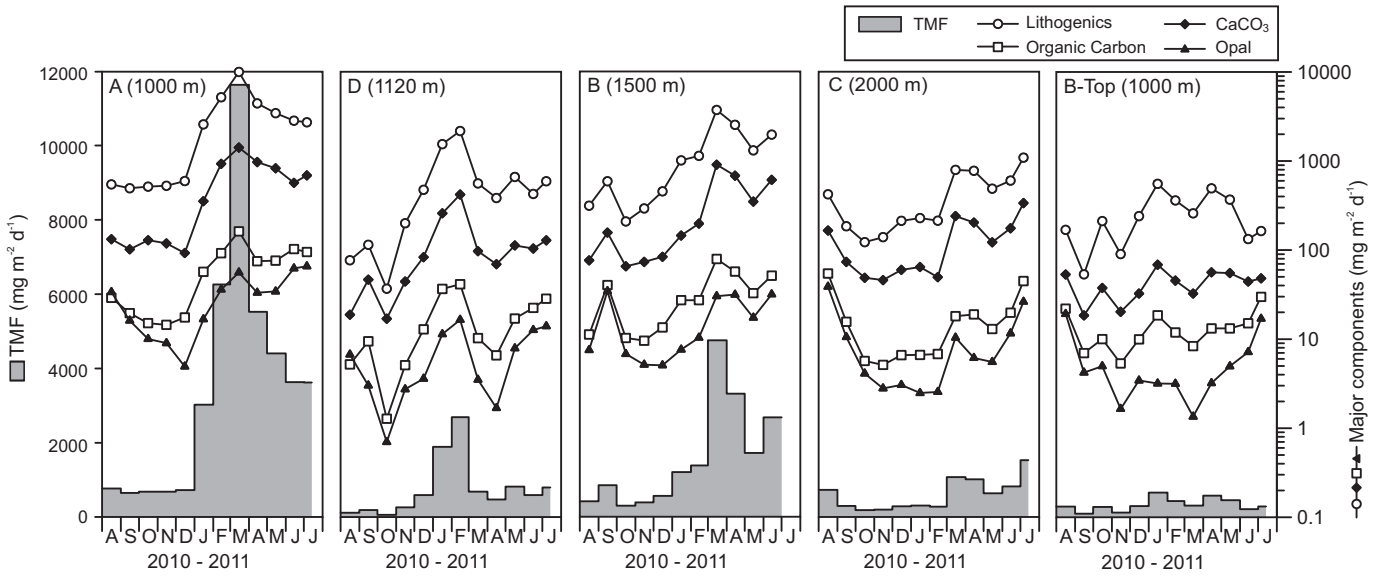

Figure 8

Click here to download Figure: FIGURE 8.pdf

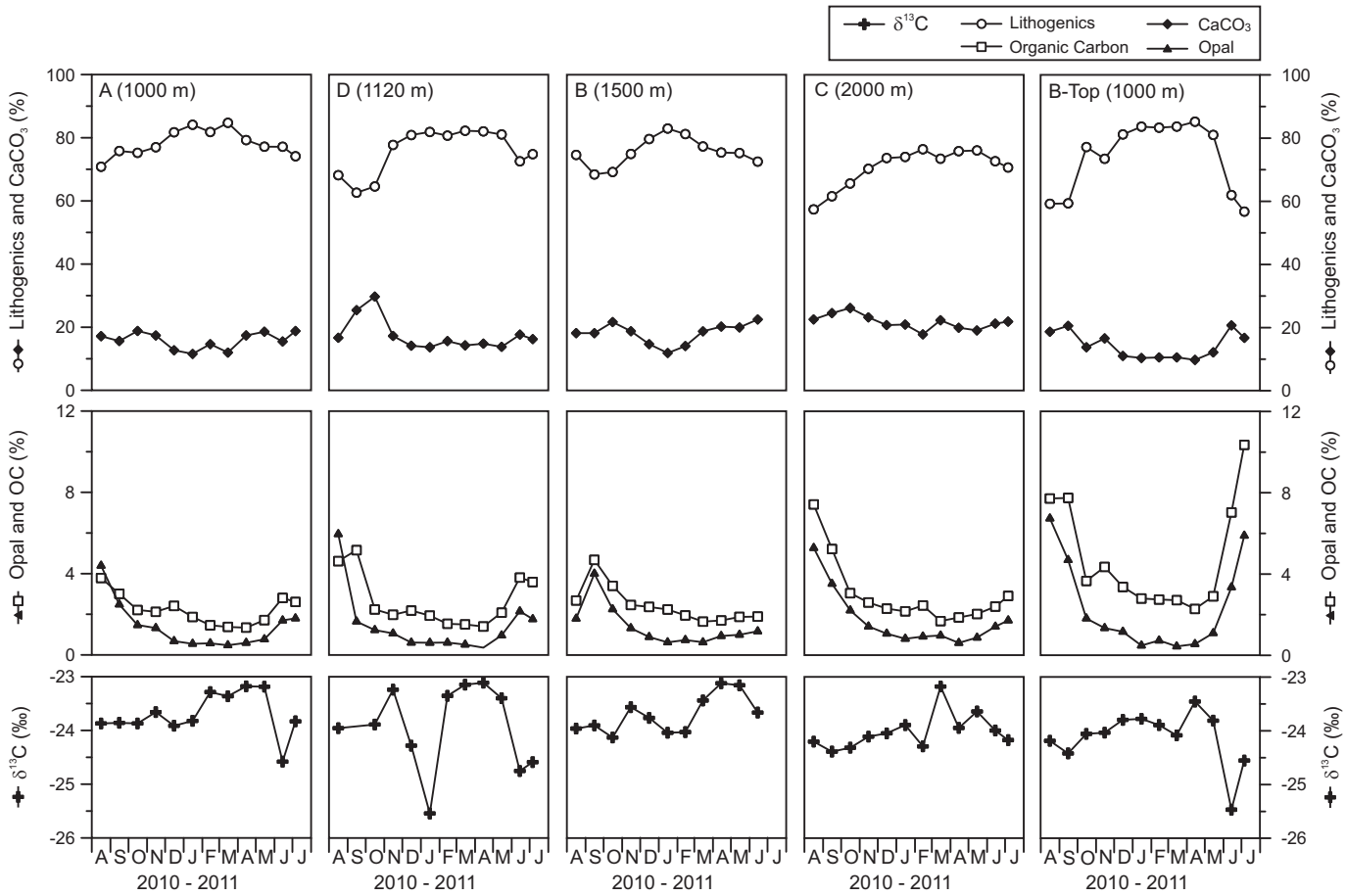

Figure 9
Click here to download Figure: FIGURE 9.pdf

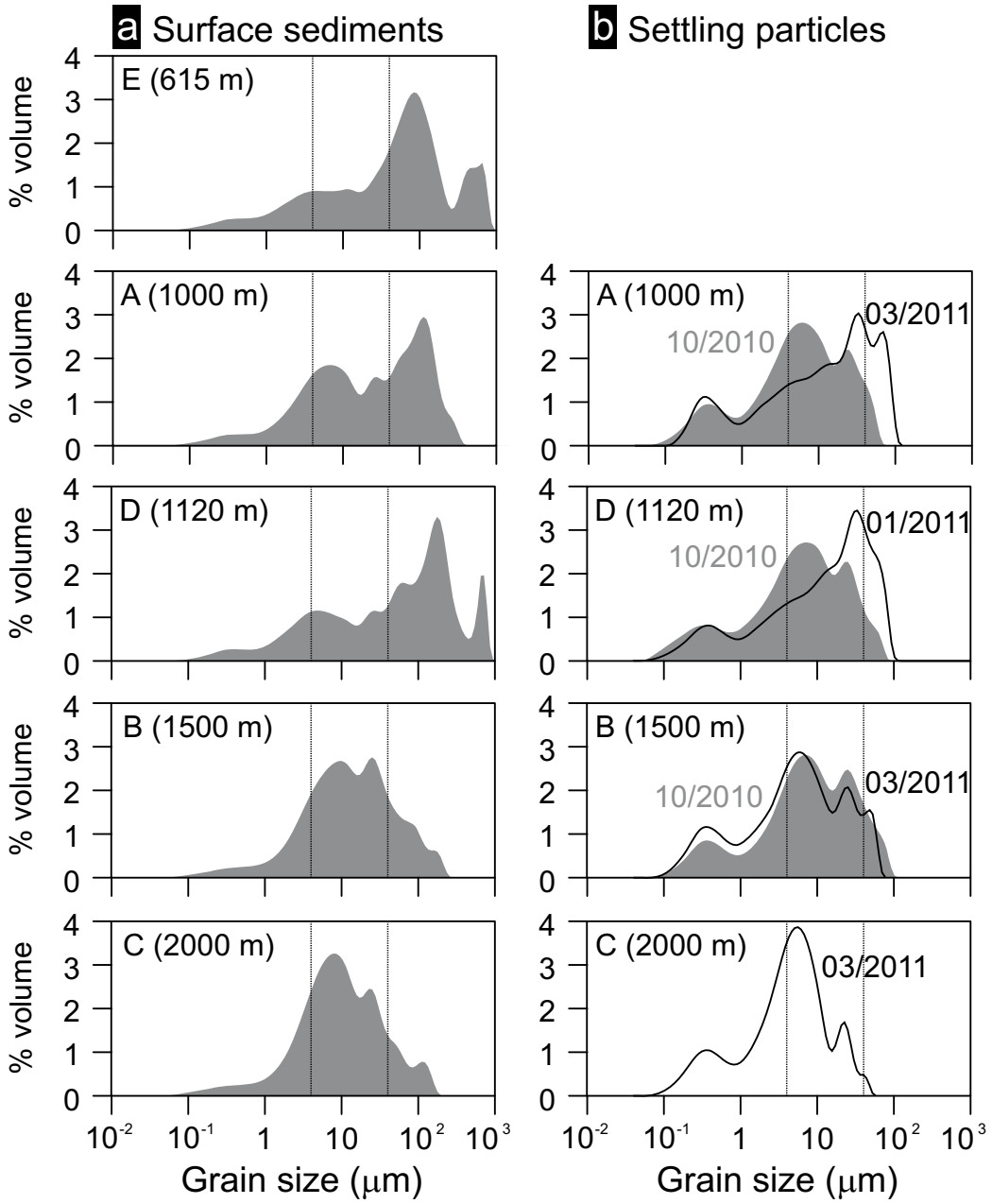

Figure 10

Click here to download Figure: FIGURE 10.pdf